Journal of
Composites Science

MDPI

Article

Effect of Biobased SiO_2 on the Morphological, Thermal, Mechanical, Rheological, and Permeability Properties of PLLA/PEG/SiO_2 Biocomposites

Johanna Morales [1,2], Rose Mary Michell [1], Alicia Sommer-Márquez [1] and Denis Rodrigue [2,*]

[1] School of Chemical Sciences and Engineering, Yachay Tech University, Urcuquí 100119, Ecuador
[2] Department of Chemical Engineering, Université Laval, Quebec, QC G1V 0A6, Canada
* Correspondence: denis.rodrigue@gch.ulaval.ca

Abstract: Nowadays, companies and researchers are concerned about the negative consequences of using synthetic polymers and direct their efforts to create new alternatives such as biocomposites. This study investigated the effect of biobased SiO_2 on the properties of poly(L-lactic acid)/SiO_2 (PLLA/SiO_2) and poly(L-lactic acid)/SiO_2/poly(ethylene glycol) (PLLA/SiO_2/PEG) composites. The SiO_2 was obtained from rice husk incineration and mixed with PLLA at various concentrations (5, 10, and 15 wt.%) via melt extrusion before compression molding. Furthermore, PLLA/SiO_2/PEG composites with various PEG concentrations (0, 3, 5, and 10 wt.%) with 10 wt.% SiO_2 were produced. The sample morphology was studied by scanning electron microscopy (SEM) to analyze the dispersion/adhesion of SiO_2 in the polymer matrix and differential scanning calorimetry (DSC) was used under isothermal and non-isothermal conditions to study the thermal properties of the samples, which was complemented by thermal stability study using thermogravimetric analysis (TGA). Rheological analysis was performed to investigate the viscoelastic behavior of the composites in the melt state. At the same time, tensile mechanical properties were obtained at room temperature to determine their properties in the solid state. DSC and X-ray diffraction analysis (XRD) were combined to determine the crystalline state of the samples. Finally, gas permeation measurements were performed using a variable pressure (constant volume) method to analyze the permeability of different gases (CO_2, CH_4, O_2, and H_2). The results showed that SiO_2 decreased the PLLA chain mobility, slowing the crystallization process and lowering the gas permeability while increasing Young's modulus, thermal stability, and viscosity. However, PEG addition increased the crystallization rate compared to the neat PLLA (+40%), and its elongation at break (+26%), leading to more flexible/ductile samples. Due to improved silica dispersion and PLLA chain mobility, the material's viscosity and gas permeability (+50%) were also improved with PEG addition. This research uses material considered as waste to improve the properties of PLA, obtaining a material with the potential to be used for packaging.

Keywords: poly(L-lactide acid); rice husk silica; poly(ethylene glycol); crystallization; tensile properties; gas permeability

Citation: Morales, J.; Michell, R.M.; Sommer-Márquez, A.; Rodrigue, D. Effect of Biobased SiO_2 on the Morphological, Thermal, Mechanical, Rheological and Permeability Properties of PLLA/PEG/SiO_2 Biocomposites. *J. Compos. Sci.* **2023**, *7*, 150. https://doi.org/10.3390/jcs7040150

Academic Editor: Francesco Tornabene

Received: 4 February 2023
Revised: 11 March 2023
Accepted: 4 April 2023
Published: 8 April 2023

1. Introduction

Over the last decades, the use of conventional petroleum-derived plastics has been less attractive because of their environmental issues. Several nations and states are banning plastic shopping bags and single-use plastics, which are considered the origin of so-called "white pollution" [1]. Therefore, the use and demand for biodegradable polymers have increased worldwide. One of the alternatives for commodity polymers is poly(lactic acid) (PLA). This polymer has several advantages, including biodegradability, biocompatibility, and a semi-crystalline structure [2–4]. This biodegradable polymer is made of renewable sources and produced by fermentation of simple sugars such as glucose, maltose, and dextrose from corn and potato starch, sucrose from cane, and lactose from cheese whey [5–7].

PLA has gained attention as a promising environmentally friendly packaging application reducing the use of petroleum-based commodity polymers [8,9]. However, PLA has some limitations restricting its applications. For example, PLA is a brittle polymer with a slow crystallization rate, poor toughness, average permeability properties, and moderate degradation [10]. Nevertheless, several modifications can be applied to enhance PLA's properties, including copolymerization [11,12], particle addition [13,14], polymer blending [15,16], and plasticization [13,15–17]. The trend and development of environmentally friendly materials led to studies and research on new production techniques for biodegradable materials using PLA as a sugarcane-based thermoplastic [18], as well as lignin addition [19] for the production of materials with good mechanical properties, excellent thermostability, and biodegradability.

In order to have a comparison of the mechanical properties of PLA with synthetic polymers, it is important to study the effect of different particles in synthetic polymers. Zaghloul et al. studied the effect of various fillers such as synthetic graphite and multi-walled carbon nanotubes (MWCNTs) [20], e-glass fiber [21,22], magnesium hydroxide [23], and melamine phosphate [24] on synthetic polymers: polyester [21,22,25], polypropylene [20], polyethylene [23,24], and polyaniline [26]. One of the conclusions of particle incorporation generated an improvement in the mechanical properties of the materials. For example, in [21–23,27], it was concluded that the tensile strength of the composites increased as the particle content increases up to an optimal amount between 16.82% [22] to almost 200% [24]. Likewise, the material's stiffness increased whereas the elongation at break decreased. In addition to the usual ways in which PLLA composites are prepared, pultruded fiber-reinforced polymers (FRP) could be explored to obtain a building material from filler or fibers and biodegradable polymers. The pultrusion manufacturing process is the most economical of all currently used methods and the benefits of FRP include high strength-to-weight ratio, increased durability, resistance to corrosion, and environmental effects, and ease of handling [28–30]. Furthermore, FRPs have been widely used in several building structures and infrastructure domains due to their exceptional properties, including flexibility, high strength, and chemical resistance [31–33]. For these reasons, pultruded FRP would be an interesting way to develop new PLLA products.

Poly(ethylene) glycol (PEG), a biocompatible and flexible polymer, is an excellent choice to modify the toughness of PLA [34]. Because the terminal hydroxyl groups in PEG molecules can react with the carboxyl groups in PLA, PEG exhibits very good miscibility with PLA [8]. Jacobsen and Fritz [35] observed that adding PEG to PLA reduced both tensile strength and elastic modulus while increasing the elongation at the break. The addition of 10 wt.% PEG increased the impact resistance by five times compared to the neat PLA. However, it is essential to understand that PLA improvements via PEG addition are limited. Sheth et al. [36] reported that PLA/PEG blends ranged from completely miscible to moderately miscible depending on the PEG content. The compounds had higher elongation at break and lower elastic modulus when the PEG content was less than 50% by weight. However, beyond 50% PEG, the morphology of the samples was altered as PEG crystallinity increased leading to higher modulus and a corresponding drop in elongation at the break. Due to the chemical nature of PEG, the crystallinity of PLA increases, whereas the cold crystallization temperature, glass transition temperature, and melting temperature decrease, thus increasing the crystallization rate [15].

Another way to modify the PLA properties is by adding fillers. Biobased particles are of interest for keeping the sustainable nature of the final compounds. Some drawbacks have been found in using agricultural waste to fill materials. The thermal stability of organic wastes such as grape stem, hemp hurd powder, hemp hurd chips, and alfalfa is lower than inorganic ones. Thus, selecting the polymer matrix with appropriate processing temperatures is mandatory to avoid the filler's decomposition [37,38]. On the other hand, inorganic fillers from waste, such as $CaCO_3$ from eggshells [39], SiO_2 from rice husk [40], and biochar from food waste [41] have higher thermal stability, which increases the thermal stability of the biocomposite. However, the tensile strength and elongation at break

decrease when a high amount of filler is added to the polymeric matrix due to particle agglomeration. Despite these limitations, the use of agricultural waste fillers is a research topic that continues to attract the attention of researchers due to its advantages: renewability, high specific resistance, low density, lightweight, and low environmental impact during production [42,43]. One example of such agricultural filler is silica (SiO_2) obtained from rice husks which contain over 20% of SiO_2 [44]. After milling rice, rice husks are often discarded, landfilled, or burned [45]. To solve this issue of a high amount of residue generation, research incorporating rice husk silica as reinforcement for agricultural filler-reinforced PLA composites has gained significant attention in the literature [14,40,46–51]. Prapruddivongs et al. [14] studied the biodegradation behavior of PLA. They crosslinked PLA filled with precipitated SiO_2 (commercial SiO_2) and SiO_2 from rice husk ash and found that SiO_2 incorporation has a direct effect on the composites' stability. In particular, introducing commercial SiO_2 in PLA and crosslinked PLA increased the degree and rate of biodegradation. According to Opaprakasit et al. [50], PLA/silica composites can improve gas permeability and selectivity. They also reported that the materials had a strong potential to be used as biodegradable packaging films with tunable gas permeability. Furthermore, the materials preserved their biodegradability because the silica particles were generated from biobased resources. Similarly, Battegazzore et al. [48] observed that the presence of extracted silica (5, 10, 20, and 30 wt.%) in PLA resulted in significant increases in Young's modulus (+32%) and a slight decrease in the oxygen permeability (−19%). Several other studies reported the effect of silica on the mechanical properties, permeability to water vapor and oxygen, as well as thermal degradation and flame retardant behavior of PLA [27,40,52–54]. Aydin and Geyikçi [47] reported that PLA/PEG/SiO_2 films had improved thermal stability (+23%) and water absorption capacity (+50%) with increasing silica concentration. Although biobased silica from rice husk is known to act as a functional filler in polymers by improving several properties, a comprehensive and comparative study on the effect of rice husk silica in PLA with PEG addition has yet to be conducted. Thus, the first part of this study investigates the effect of rice husk SiO_2 content on the properties of PLLA/SiO_2 composites. Then, PLLA/SiO_2/PEG composites are studied to determine the effect of PEG on the final properties.

2. Materials and Methods

2.1. Materials

The rice husk was a residue of rice milling (Retsch, Haan, Germany), whereas the PLLA (4043D), with 94% l-lactide and 6% d-lactide content. The properties of PLLA (4043D) are shown in Table 1, was supplied by Ingeo Nature Works (Blair, NE, USA). The PEG selected had a molecular weight (Mw) of 6000 g/mole and purchased from Merck Millipore (Burlington, MA, USA). The properties of PEG 6000 are presented in Table 2. Hydrochloric acid (37%) was obtained from Sigma-Aldrich (Burlington, MA, USA).

Table 1. Physical and mechanical properties of PLLA (4043D).

Property	Value	ASTM Method
Relative viscosity	4.0	D5225
Peak melt temperature	145–160 °C	D3418
Glass transition temperature	55–60 °C	D3418
Tensile yield strength	8700 (60) psi (MPa)	D882
Tensile strength at break	7700 (53) psi (MPa)	D882
Tensile modulus	524,000 (3.6) psi (MPa)	D882
Tensile elongation	6%	D882

Table 2. Physical and chemical properties of PEG 6000 g/mol.

Property	Value
Density	1.2 g/cm^3 at 20 °C
Peak melt temperature	145–160 °C
Melting range	59–64 °C
Hydroxyl value	16–23
Average molecular mass	5000–7000 g/mol

2.1.1. SiO_2 Preparation

The rice husk was first ground with an industrial mill (Retsch, Haan, Germany) and then washed with a solution of HCl 1 M for 2 h before being washed with distilled water up to 10 times until the solution pH was neutral. Then, the rice husk was placed overnight in an oven at 60 °C for drying. Finally, the material was left at 600 °C for 7 h to obtain amorphous SiO_2. The process for obtaining SiO_2 from rice husk was based on previous work [44,47,48]; typical properties of the silica obtained are described in Table 3.

Table 3. Characteristics of SiO_2 extracted from rice husk.

Property	Value
Average particle size	10–40 µm
Content of carbon (C)	21.25% of mass
Content of oxygen (O)	45.41% of mass
Content of silicon (Si)	33.34% of mass

2.1.2. Composites Preparation

Grounded PLLA and SiO_2 were pre-dried for 2 h at 60 °C to remove the residual moisture content. Mixing of PLLA, PEG, and SiO_2 was performed manually (dry-blending of the powders) at different concentrations before being melt-blended in a co-rotating twin-screw extruder (Leistritz ZSE-27, Nürnberg, Germany) with an L/D ratio of 40 and 10 heating zones (die diameter of 2.7 mm). The total flow rate was 0.5 kg/h and the screw speed was fixed at 70 rpm. Because PLLA exhibits its maximum melting temperature between 175 and 180 °C [55], the temperature profile imposed was 175 °C for the first zone (feed), 190 °C for the second to the eighth zone, 170 °C for the ninth zone, and 150 °C for the tenth zone (die) to limit degradation. At tap water temperature (10–15 °C), PLA is in a solid state below its T_g which is between 55 and 60 °C [56]. Therefore, tap water was used for the water bath to promote an eco-friendly process without any modifications. In contrast, higher temperatures near T_g will affect the composites' final properties, increasing the material's brittleness and stiffness [57,58]. Then, the filament was pelletized using a model 304 pelletizer (Conair, CA, USA) to be finally dried at 60 °C for 2 h to remove any remaining water. All the compositions investigated are presented in Table 4. The elaboration process of the composites was designed based on previous work [15,40,49,59] and prevents material degradation processes.

Table 4. Formulations for the composites.

Samples	PLLA (wt.%)	SiO_2 (wt.%)	PEG (wt.%)
PLLA	100	-	-
PLLA/SiO_2 (95/5)	95	5	-
PLLA/SiO_2 (90/10)	90	10	-
PLLA/SiO_2 (85/15)	85	15	-
PLLA/SiO_2/PEG (90/10/3)	90	10	3
PLLA/SiO_2/PEG (90/10/5)	90	10	5
PLLA/SiO_2/PEG (90/10/8)	90	10	8
PLLA/SiO_2/PEG (90/10/10)	90	10	10

2.2. Methods

2.2.1. Morphology

An Inspect F50 scanning electron microscope (SEM) (FEI, Hillsboro, OR, USA) was used at 10 kV to take images of the SiO_2 particle. After cryogenic fracture, a lower voltage (2–5 kV) was used to take micrographs of the PLLA and PLLA composite cross-sections. The samples were cut with a sharp knife in both the flow (F) and transverse (T) directions to provide a thorough 3D characterization of the deformed cellular structure caused by the cryogenic rupture. In addition, a thin Au/Pd coating was applied on the exposed surfaces. Energy dispersive spectroscopy (EDS) was also used to study the SiO_2 composition and to identify contaminants. The system used was an Edax Ametek Model Octane Super-A.

2.2.2. Differential Scanning Calorimetry

A DSC-8 Perkin Elmer (Waltham, MA, USA) differential scanning calorimeter connected to a cooling system calibrated with pure indium and tin standards was used with the Pyris software. Samples of about 5 mg, sealed in aluminum pans, were used. All the experiments were performed under an N_2 atmosphere with a flow rate of 20 mL/min. For the non-isothermal cold crystallization determination, the samples were melted at 200 °C. The thermal history of the samples was erased by holding the temperature for 3 min before being cooled down from the melting state to 0 °C at a rate of 10 °C/min. Finally, the samples were heated back to 200 °C at 10 °C/ min. The degree of crystallinity (X_c) was calculated as:

$$X_c(\%) = \left(\frac{\Delta H_m - \Delta H_{cc}}{\Delta H_m^0}\right)\left(\frac{1}{w}\right)(100\%) \quad (1)$$

where ΔH_m is the experimental heat of fusion (J/g), ΔH_m^0 is the theoretical heat of fusion of the 100% crystalline PLLA (93 J/g) [60], and w is the weight fraction (wt/wt) of PLLA in the composites.

2.2.3. Equilibrium Melting Temperature Determination

The Hoffman–Weeks (HW) method involves the extrapolation of a linear regression of experimentally observed melting temperatures (T_m) for various crystallization temperatures (T_c) to the equilibrium line ($T_m = T_c$). After isothermal crystallization, the samples were heated to 200 °C, and the equilibrium melting temperature (T_m^0) was calculated by extrapolating the first fusion peak to the intersection of $T_m = T_c$.

2.2.4. Isothermal Crystallization

After erasing the thermal history for 3 min at 200 °C, samples of about 5 mg were rapidly cooled down from the melting state to 0 °C (about 80 °C/min) to prevent crystallization during cooling. The samples were then heated to the selected crystallization temperature. The exothermic crystallization was recorded as a function of time until equilibrium was achieved (about three times the half-crystallization duration). The samples were then heated at a rate of 20 °C/min to record the melting behavior of the isothermally crystallized composite. Preliminary tests were performed to identify the appropriate crystallization temperatures (T_c). The samples were rapidly cooled down from the melting point (about 80 °C/min) to a predetermined T_c and then heated at 20 °C/min to determine whether any melting could be observed. Then, a test with a more precise T_c was carried out until no crystallization occurred during the previous cooling. A T_c temperature range including at least six different temperatures was used [61].

2.2.5. Thermogravimetric Analysis

The weight curves (TGA) were recorded using a TA Instruments (New Castle, DE, USA) model Q5000IR from 30 to 600 °C at a heating rate of 10 °C/min under a nitrogen atmosphere (25 mL/min).

2.2.6. Melt Rheology

An ARES (TA Instruments, New Castle, DE, USA) rotational rheometer with 25 mm discs and a 3 mm gap was used to characterize the viscoelastic properties in the melt state. All experiments were carried out at 190 °C under a nitrogen atmosphere. After performing dynamic strain sweeps to determine the limits of the linear viscoelastic range, frequency sweeps were performed at a strain of 7%. The data obtained analyzed the elastic modulus, loss modulus, complex viscosity, and damping factor (tan (δ)) to quantify the rheological properties in the melt state.

2.2.7. Tensile Test

Tensile tests were performed at room temperature using an Instron 5565 universal machine and Blue Hill software following ASTM D882. Rectangular samples (length = 10 cm, width = 0.5 cm) were cut and examined at 2 mm/min. The average values of the mechanical properties with the corresponding standard deviation have been measured for five specimens. Tensile modulus, tensile strength, and elongation at break were the outcomes of the test.

2.2.8. X-ray Diffraction Analysis

An X-ray diffractometer Rigaku with D/tex ultra 2 detectors was used to obtain the patterns. The measurement conditions were 30 kV and 20 mA for the X-ray generator in a sealed tube with a Cu K$\alpha_{1,2}$ radiation source. For collecting the data, the angular region selected was 2θ = 5–90° with a step size of 0.005°. The crystallization degree was calculated using the Match! Program. Before carrying out the measurements, the samples were placed in holders and then heated for one hour at 80 °C in a vacuum oven.

2.2.9. Gas Permeation Measurements

The membranes were tested for pure gases (N_2, O_2, CO_2, and CH_4). The pure gas transport properties were measured using a variable pressure (constant volume) method [62]. For pure gases, the permeability coefficient P (cm^3 (STP) cm/cm^2 s cmHg) was calculated as:

$$P = \frac{22414}{A}\frac{V}{RT}\frac{l}{\Delta p}\frac{dp}{dt} \quad (2)$$

where A is the membrane area (cm^2); l is the membrane thickness (cm); Δp is the upstream pressure (psi); V is the downstream volume (cm^3); R is the universal gas constant (6236.56 cm^3 cmHg/mol K); T is the absolute temperature (K) and dp/dt is the permeation rate (psi/s). The permeabilities are reported with units of Barrer (10^{-10} cm^3 (STP) $cm/(cm^2$ s cmHg)). All the permeation measurements were performed at the same temperature (°C) and feed pressure (40 psi).

3. Results

3.1. Morphology

The extraction of SiO_2 from the rice husk is a fundamental part of our study, which is why studying the purity of the silica obtained is important. Figure 1 shows that the EDS spectrum contains peaks corresponding to silicon and oxygen, indicating that the particles obtained are mostly silica.

The analysis of the interaction between the polymeric matrix and the filler, as well as the miscibility of PEG in the PLA matrix, is important because the PLA's physical, mechanical, and barrier properties are affected by its morphology [63]. Figure 2a presents the amorphous SiO_2 particles extracted from rice husks with particle sizes (diameter) distribution from 10 to 40 micrometers. Figure 2b shows that neat PLLA has a homogenous surface with surface fractures highlighting the material's fragility [64]. For the composites, Figure 2c–e shows that the SiO_2 particles are uniformly distributed without interfacial decohesion, indicating that good mixing conditions were used and that strong interac-

tions between both materials were obtained since no voids/defects can be seen. Finally, Figure 2f–i present micrographs of the composites with PEG. Compared to PLLA/SiO_2 composites, the PLLA/SiO_2/PEG samples exhibit a much smoother surface (less brittle) and a better silica particle distribution. Because both PLLA and PEG contain significant amounts of hydroxyl groups, they are expected to be compatible between themselves and with the polar SiO_2 particles leading to homogeneous samples as presented here [65].

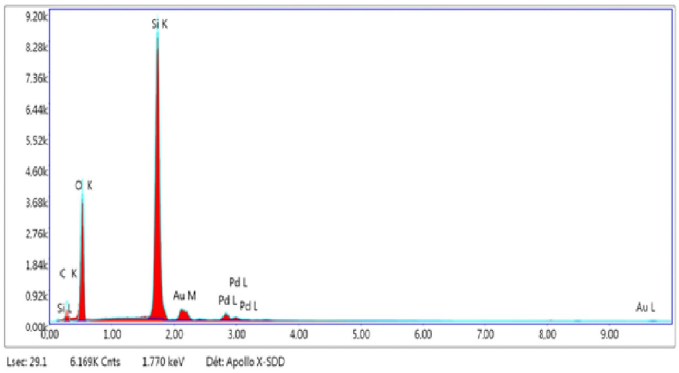

Figure 1. EDS spectra of the SiO_2 particles showing the composition (purity) of the sample.

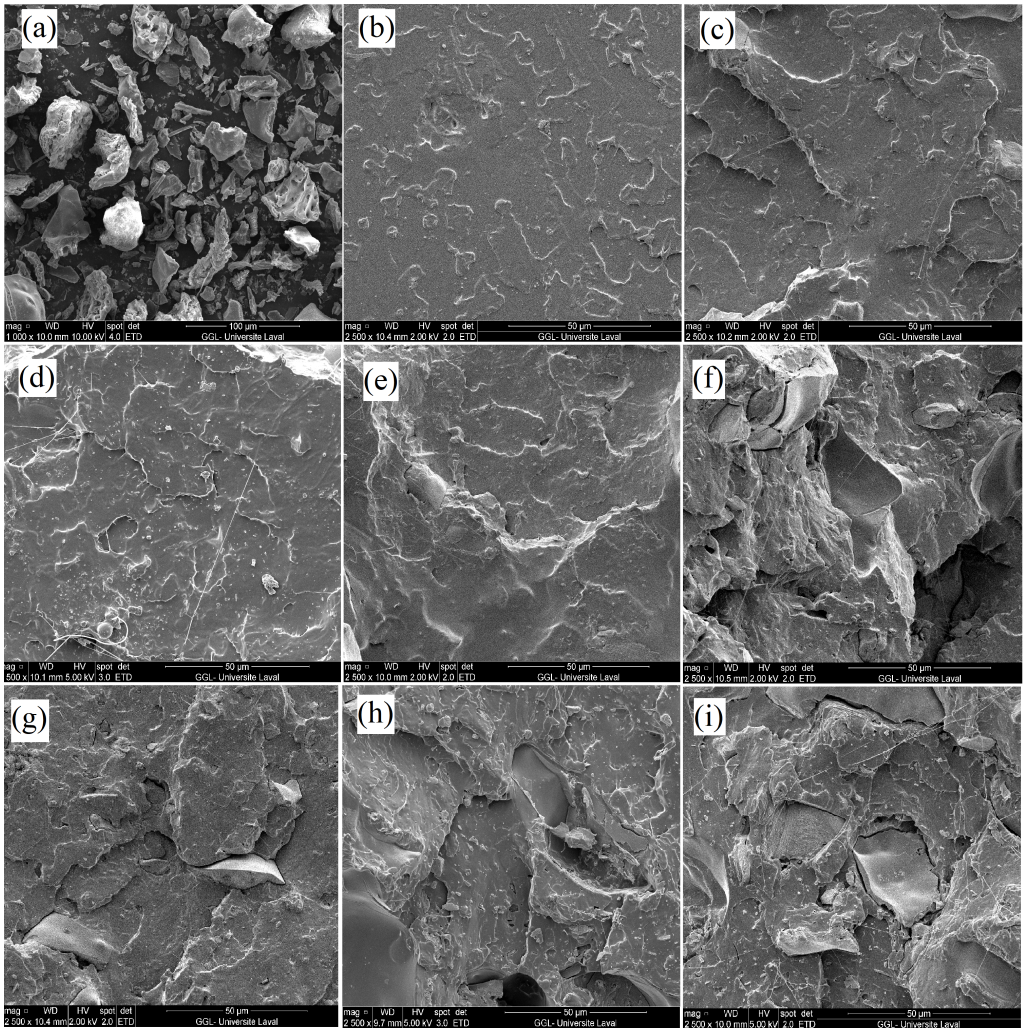

Figure 2. SEM micrographs of: (**a**) SiO_2 from rice husk, (**b**) neat PLLA, (**c**) PLLA/SiO_2 (95/5), (**d**) PLLA/SiO_2 (90/10), (**e**) PLLA/SiO_2 (85/15), (**f**) PLLA/SiO_2/PEG (90/10/3), (**g**) PLLA/SiO_2/PEG (90/10/5), (**h**) PLLA/SiO_2/PEG (90/10/8), and (**i**) PLLA/SiO_2/PEG (90/10/10).

3.2. Differential Scanning Calorimetry

3.2.1. Non-Isothermal Crystallization

To determine the effect of SiO_2 particles on the order/spatial distribution of PLLA chains was the main goal of their addition into PLLA. This is why the analysis is focused on the crystallization process of these composites. The DSC thermograms for the first heating and cooling of the composites are presented in the supplementary information as Figure S1a,b, respectively. Figure S1a shows a slight decrease in the glass transition temperature (T_g) and cold crystallization temperature (T_{cc}) for composites with 5 and 10% of silica due to the previous crystallization temperature. Furthermore, no change in the melting temperature (T_m) is observed since, for the first and second heating steps, the value is close to 150 °C. Two melting peaks are observed, and changes in the peak melting temperature are explained in the second heating analysis. On the other hand, Figure S1b shows no crystallization peak; only a glass transition temperature of around 60 °C, as expected for polyesters.

The second heating thermograms are presented in Figure 3. The cold crystallization behavior is typical of aliphatic polyesters such as PLA. It reflects the material's ability to crystallize below the melting temperature [66]. Because crystallization occurs during the heating scan, an increase in T_{cc} for PLLA/SiO_2 (85/15) is related to more difficulty in chain mobility hindering the PLLA crystallization [67]. Then, a melting process occurs as determined by the presence of two melting peaks. The melt-recrystallization model states that the exothermic peak occurs when the recrystallization rate exceeds the melting rate.

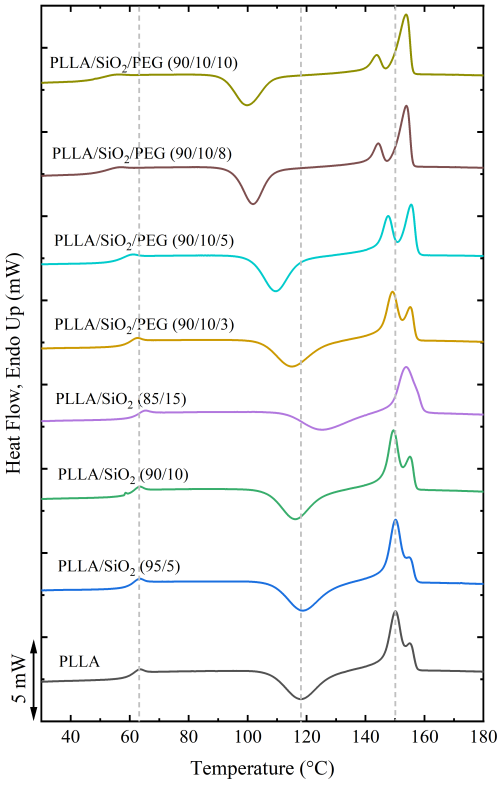

Figure 3. Thermogram of the second DSC heating step for PLLA, PLLA/SiO_2, and PLLA/SiO_2/PEG.

Silica, at high concentrations, makes recrystallization more challenging (less space and more limitation), as confirmed by a single fusion peak for the highest silica concentration. In contrast, the endothermic peak occurs when the melting rate overcomes recrystallization [4,68,69]. This lower temperature peak can also be related to the melting of α'-crystals and their recrystallization into the α crystalline form [70].

In order to improve the silica dispersion in the PLLA matrix, different amounts of PEG were added to evaluate the crystallization rate and the interaction with PLLA/SiO_2. The

value of T_g is an excellent indicator of the polymer structure and chain mobility [71]. As shown in Figure 3, the T_g decreases with increasing PEG content compared to neat PLLA, showing good miscibility between the polymeric matrix and the plasticizer [72]. The T_{cc} and T_g both decrease with increasing PEG content since PLLA crystallizes more easily due to increased chain mobility [71] and chain packing [73]. As a result, Table 5 shows that by increasing the PEG content, the degree of crystallinity increases by 90% compared to neat PLLA and by up to 40% compared with the composite having 10 wt.% silica.

Table 5. Enthalpy of fusion, glass transition, melting temperature, and degree of crystallinity from the second heating step at 10 °C/min.

Sample	T_{cc} (°C)	ΔH_{cc} (J/g)	T_g (°C)	T_m (°C)	ΔH_m (J/g)	X_c (%)
PLLA	118.0	−23.8	59.9	150.1/155.1	26.9	3.4
PLLA/SiO_2 (95/5)	118.7	−25.2	59.9	150.2/155.0	27.2	2.3
PLLA/SiO_2 (90/10)	116.1	−22.5	59.9	149.5/155.1	26.4	4.6
PLLA/SiO_2 (85/15)	125.2	−17.6	61.8	153.8	21.3	4.7
PLLA/SiO_2/PEG (90/10/3)	115.0	−23.3	58.8	149.1/155.2	25.2	2.3
PLLA/SiO_2/PEG (90/10/5)	109.5	−24.6	56.3	147.6/155.5	27.6	3.8
PLLA/SiO_2/PEG (90/10/8)	101.8	−23.2	51.2	144.3/153.8	28.2	6.4
PLLA/SiO_2/PEG (90/10/10)	99.8	−23.3	49.6	143.8/153.7	28.2	6.5

3.2.2. Isothermal Crystallization

Equilibrium Melting Temperature Determination

Figure 4a presents a typical example of DSC heating scans for PLLA/SiO_2 (90/10). For the different isothermal crystallization temperatures used, two melting peaks were identified. T_m^0 is often calculated by linearly extrapolating the T_m vs. T_c plot to the line $T_m = T_c$, as stated by linear Hoffman–Weeks (HW) extrapolation shown in Figure 4b. The values of the T_m^0 obtained for all samples are reported in Table 6. The reference T_m^0 is taken from the literature as 207 and 206 °C [74–76]. Different trends in T_m^0 are observed: for the composites with silica alone, the value decreases from 180 to 175 °C at 10 wt.%, whereas it increases to 184 °C at 15 wt.%. It is known that T_g and T_m^0 are the main factors influencing the crystallization rate of a polymer [8]. Because of the high silica concentration added, T_m^0 increases. As a result, nucleation is favored. Even if these T_m^0 values are lower than those reported in the literature, the thickening ratio (γ) exhibits a typical value between 2 and 3 by linear HW extrapolation [77]. It can be concluded that the linear HW extrapolation is valid to determine the T_m^0 of our PLLA composites. Furthermore, T_m^0 for the composites containing silica and PEG increase with PEG content: from 169 to 215 °C. This increase in T_m^0 is expected since, as reported in Table 5, the presence of PEG improves the crystallization rate by increasing the crystallization's driving force; i.e., chain mobility [8]. For the values of γ, no variation is observed in the composites containing silica. However, a decreasing trend is observed with PEG, implying that lower lamellar thickness is needed to activate secondary surface nucleation and growth.

Table 6. Variation of T_m^0 with SiO_2 and PEG content, as determined by the Hoffman–Weeks extrapolation procedure.

Samples	T_m^0 (°C)	γ (-)
PLLA	180	2.4
PLLA/SiO_2 (95/5)	180	2.4
PLLA/SiO_2 (90/10)	175	2.6
PLLA/SiO_2 (85/15)	184	2.4
PLLA/SiO_2/PEG (90/10/3)	169	3.2
PLLA/SiO_2/PEG (90/10/5)	198	1.9
PLLA/SiO_2/PEG (90/10/8)	199	1.9
PLLA/SiO_2/PEG (90/10/10)	215	1.7

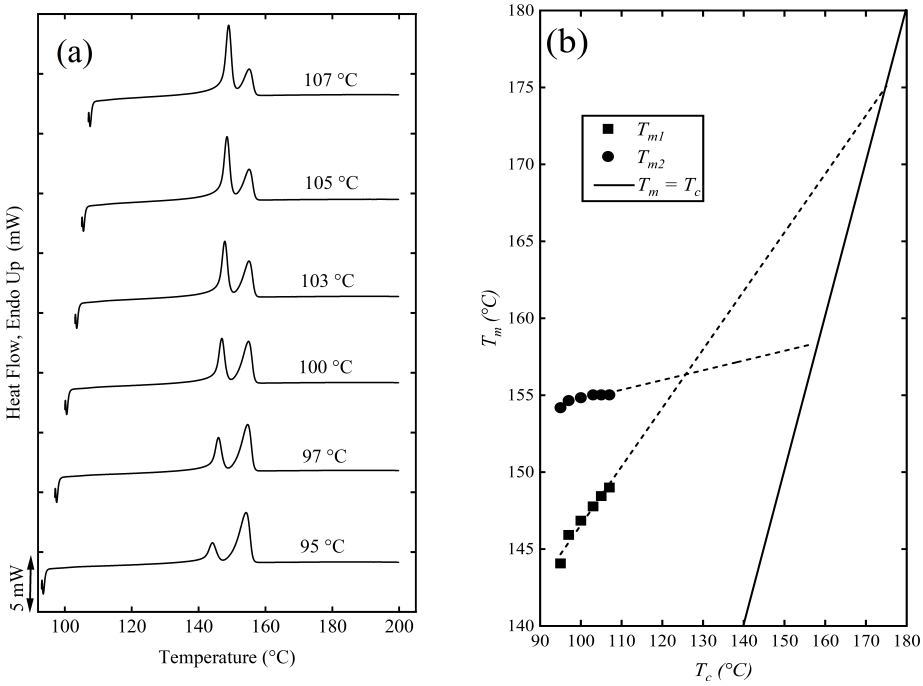

Figure 4. (**a**) DSC heating scans after isothermal crystallization at the indicated temperatures for the PLLA/SiO_2 (90/10) composite. (**b**) Hoffman–Weeks plot for the same composite.

Isothermal Crystallization Kinetics

Figure 5 presents the experimental data for the overall crystallization rate of PLLA composites as a function of isothermal crystallization temperature T_c. The T_c required for crystallization slightly increases with SiO_2 content, implying that supercooling decreases due to the filler content inhibiting the PLLA chain motion, and increasing the energy barrier for spherulite development [78]. In contrast, lower T_c is required for the crystallization of PLLA/SiO_2/PEG composites, implying an increase in supercooling. This behavior is related to the results presented in Figures 3 and 4, where PEG has high miscibility in PLLA, increasing the mobility of PLLA chains and crystallization rate. The result is an overall decrease in the crystallization rate. Furthermore, the values of half-crystallization time increase as the crystallization temperature decreases. This behavior is related to the proximity of the crystallization temperatures used since it is known that crystallization is slower near T_g and T_m.

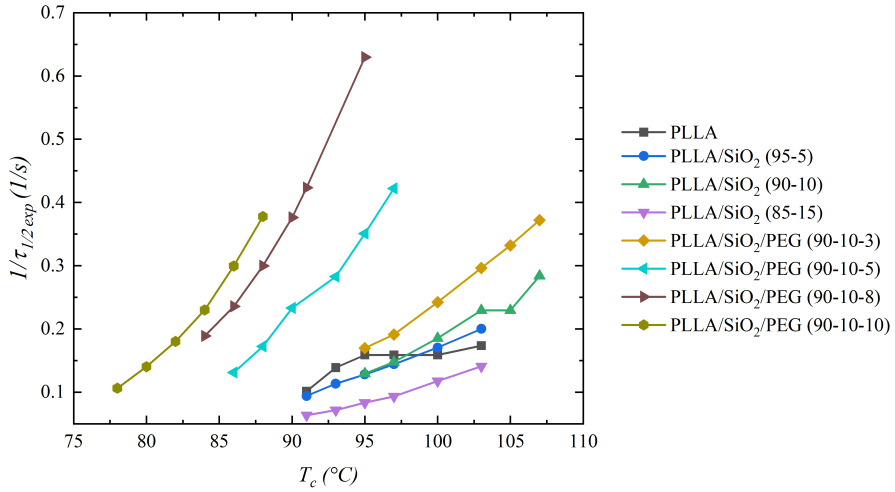

Figure 5. Values of $1/\tau_{1/2exp}$ as a function of the isothermal crystallization temperature (T_c).

Figure 6 presents the values of half-crystallization time as a function of SiO_2 and PEG content. Due to low chain mobility [63], the inverse of half-crystallization time decreases as SiO_2 content increases. On the other hand, increasing the PEG content increases the PLLA chain mobility leading to higher half-crystallization times at lower crystallization temperatures.

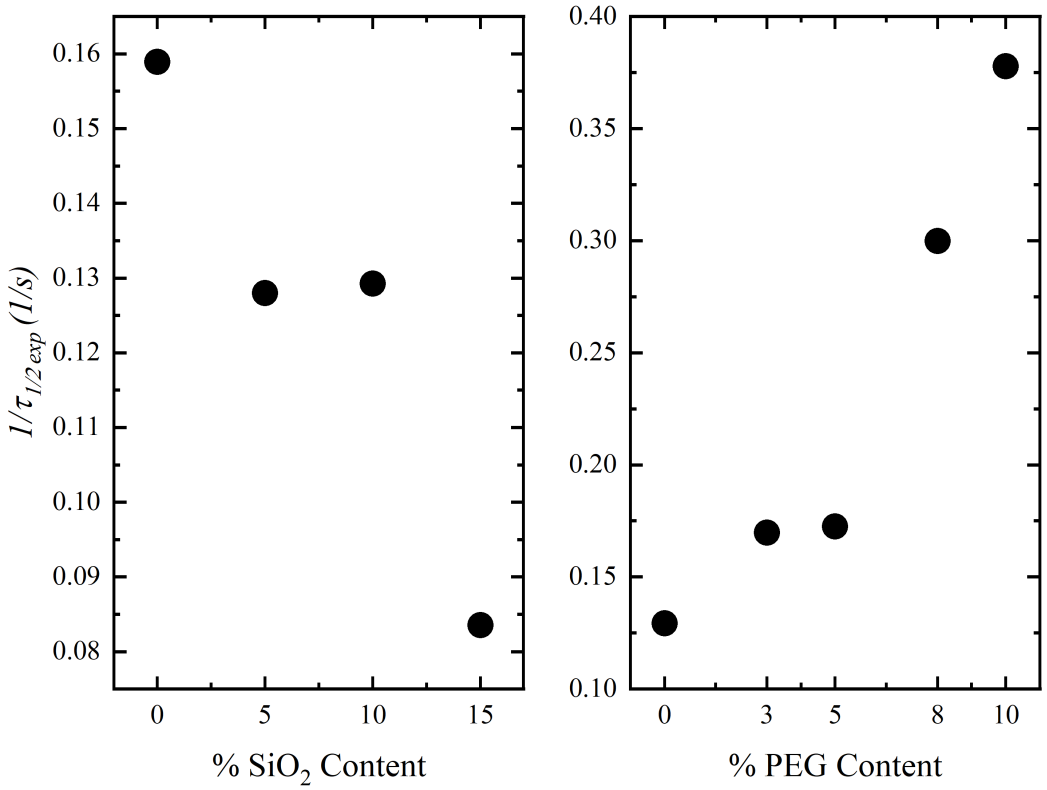

Figure 6. Values of $1/\tau_{1/2exp}$ at 95 °C for PLLA/SiO_2 and 88 °C for PLLA/SiO_2/PEG.

Avrami's theory is often used to model isothermal crystallization kinetics using overall crystallization rate data. In this work, we followed the experimental protocols and analyses established by Lorenzo et al. [61,79]. The Avrami equation can be written as:

$$1 - V_c(t) = exp(-kt^n) \quad (3)$$

where V_c is the relative volumetric transformed fraction (mg/mg), n is the Avrami index (-), and k is the overall crystallization rate constant (min^{-n}) containing contributions from nucleation and growth [61,80]. Parameters n and k can be obtained from the slope and intercept of the Avrami plot of log[$-$ln(1 $-$ X_t)] vs. log(t). Table S1 presents the results obtained from the Avrami fit. Figures S2 and S3 show that the Avrami model fits well with the experimental data up to 50% conversion. Figure S4 compares the Avrami-derived DSC curve with the experimental data where proper fitting is observed within the primary crystallization region. The values of k follow a trend similar to the one seen in Figure 5. The higher values of the isothermal crystallization parameter k reported in Table S1 confirm the increase in chain mobility related to PEG addition to PLLA/SiO_2 composites. The Avrami predicted values of half-crystallization time are very similar to the experimental values in most cases, as expected from the trends shown in Figure S2. Figure 7 presents the values of n as a function of the isothermal crystallization temperatures. These values are associated with the nucleation type during the experiment [61]. Changes in n indicate that conditions, such as the presence of a plasticizer and crystallization temperatures, strongly influence the crystallization mechanism of PLLA. Values in the range of 3–4 were obtained for PLLA/SiO_2 composites indicating that mainly heterogeneous nucleation with three-dimensional sporadic crystal growth was favored in the presence

of a filler [66] at higher crystallization temperatures (from 91 °C). In contrast, values close to 3 for PLLA/SiO_2/PEG composites indicate that a specific PEG concentration favored three-dimensional instantaneous crystal growth at lower temperatures (from 78 °C) as PEG interacts with PLLA chains increasing their mobility [81].

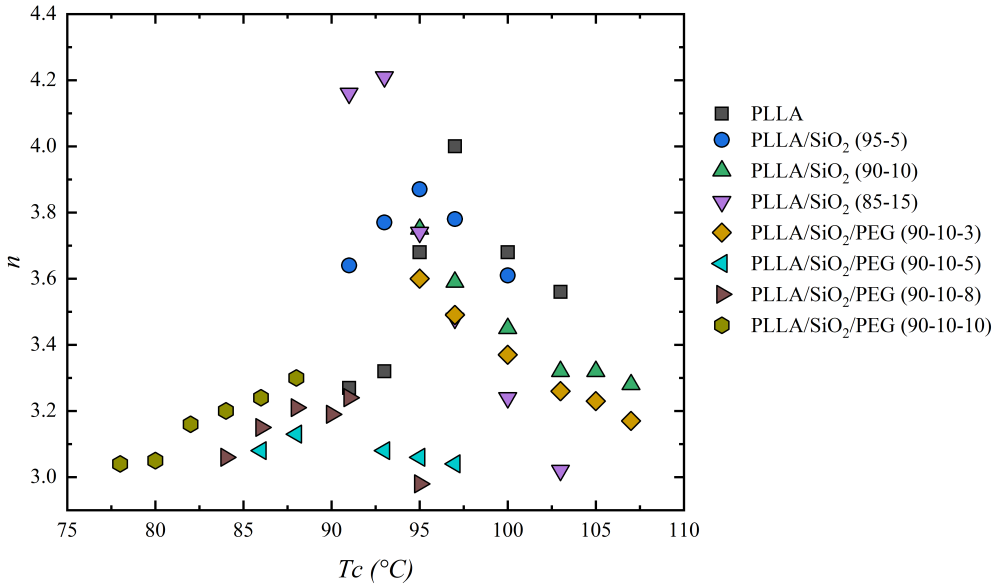

Figure 7. Avrami index (n) as a function of isothermal crystallization temperature (T_c).

The Lauritzen–Hoffman (LH) theory has been a popular technique for studying crystal growth. It is possible to analyze the observed isothermal crystallization data regarding secondary nucleation or the LH theory of polymer crystal development [4,68,74,82–84]. The growing face goes through two distinct but connected processes during polymer crystallization. In one, secondary nuclei are deposited on the growth face, whereas in the other, growth continues along the face at the locations where the secondary nuclei are created [80]. Although the actual size of the nucleus is significant in theoretical research, it is challenging to determine it physically because of the experiments' limited spatial resolution. Therefore, LH theory is a powerful tool for theoretically investigating the characteristics of secondary nucleation.

Hoffman evaluated experimental data on spherulite growth rate using the secondary nucleation theory. This led to the HL equation given by [83]:

$$G = G_0 exp\left(\frac{-U^*}{R(T_c - T_\infty)}\right) exp\left(\frac{-K_g}{T_c \Delta T f}\right) \quad (4)$$

where ΔT is the degree of supercooling defined by $T_m^0 - T_c$, T_m^0 is 480 K [75,76], f is a factor (K/K) expressed as $\left(\frac{2T_c}{T_m^0 + T_c}\right)$, U^* is the activation energy for segment diffusion to the crystallization site (1500 cal/mol = 6276 J/mol) in order to compare the results with the literature, R is the gas constant (8.314 J/(mol K)), T_∞ is the hypothetical temperature expressed as (T_g − 30 K), whereas G_0 is the front factor [(J/mol)/(J/mol)] and K_g is the nucleation constant (K^2) defined as:

$$K_g = \left(\frac{Z b_0 \sigma \sigma_e T_m^0}{\Delta h_f k_B}\right) \quad (5)$$

where σ is the lateral surface free energy (J/m^2), σ_e is the fold surface energy (J/m^2), b_0 is the crystal layer thickness (m), Δh_f is the volumetric heat of fusion (J/m^3), and k_B is the Boltzmann constant (1.380649×10^{-23} J/K) [80]. In general, the value of Z depends on the crystallization regime and equals to 4 for regimes I (high temperatures)

and III (low temperatures), whereas a value of 2 must be used for regime II (intermediate temperatures) [82]. In this work, the crystallization rate was associated with $1/\tau_{(1/2)}$ leading to $Z = 4$ for the crystallization regime. All the numerical results are reported in Table 7.

Table 7. Kinetics parameters for PLLA and the composites obtained by the HL model (Equation (4)).

Sample	K_g 10^{-5}	σ 10^{-3} (J^2/m^4)	q (kJ/mol)	Regime
PLLA	9.67	96.9	36.0	III
PLLA/SiO_2 (95/5)	8.36	83.8	31.1	III
PLLA/SiO_2 (90/10)	5.75	57.7	21.4	III
PLLA/SiO_2 (85/15)	8.03	80.5	29.9	III
PLLA/SiO_2/PEG (90/10/3)	5.18	51.9	19.2	III
PLLA/SiO_2/PEG (90/10/5)	6.17	61.9	23.0	III
PLLA/SiO_2/PEG (90/10/8)	4.54	45.5	16.9	III
PLLA/SiO_2/PEG (90/10/10)	5.18	51.9	19.2	III

For neat PLLA, the value of σ_e is 97 × 10^{-3} J/m^2 which is in the range of values reported in the literature: 43.5 × 10^{-3} J/m^2 [84] to 107 × 10^{-3} J/m^2 [76,85]. It has been shown that the value of σ_e is affected by the molecular weight of PLLA [76], as well as the cooling or heating rate of the isothermal crystallization temperature [84,85]. For the composite containing 15 wt.% silica, the value of σ_e increases indicating that excessive silica addition decreases crystallization due to the impeding effect of a high amount of rigid particles [84]. In contrast, the values of σ_e substantially decrease with PEG content, indicating that PEG acts as a plasticizer improving the nucleation and mobility of PLLA chains [78], leading to lower lamellar thickness [80].

From the values obtained for chain folding (q) (kJ/mol) and σ_e, a clear decreasing trend can be seen. These results suggest that the presence of PEG lowered the work required for PLLA chains to fold into crystals. PEG improved the PLLA chain mobility and accelerated crystallization by lowering the energy required for the chain folding process during crystallization [81,86]. However, a slight increase in q for the composites with 8 and 10 wt.% was observed. This behavior might be linked to some PEG molecules being trapped in the intraspherulitic region of PLLA, inhibiting PLLA crystallization [87].

In the HL secondary nucleation theory (Equation (4)), polymers crystallize in three distinct regimes [83]. Figures S5 and S6 show that T_c is between 78 and 107 °C, indicating that crystallization occurs in regime III. Regime III involves thin lamellar crystals developed under high undercooling and characterized by irregular surfaces. As a result, the rate is fast at low temperatures (high undercooling), and a high number of smaller nuclei are generated [88].

3.3. Thermal Stability

Thermogravimetric analysis (TGA) of PLLA, PLLA/SiO_2, and PLLA/SiO_2/PEG was used to study their thermal stability and relationship with crystallinity. Figure 8a depicts the weight curve and its derivative (DTA) in Figure 8b as a function of temperature. Figure 8a shows that the incorporation of SiO_2 increased the onset and endset temperature of the composites. Silica particles act as barriers to impede the diffusion of volatile components increasing the thermal stability [47].

On the other hand, PEG allows the chain segments to move quickly and improves the flexibility of PLLA [47,89]. Increasing the PEG content also lowers the PLLA degradation temperature because PEG has a lower thermal degradation temperature than PLLA. This behavior is more visible for composites having higher PEG content (8 and 10 wt.%), as presented in Table 8 Since silica does not show any thermal degradation up to 600 °C, the total weight lost is proportional to the amount of polymer in the composite (excluding silica).

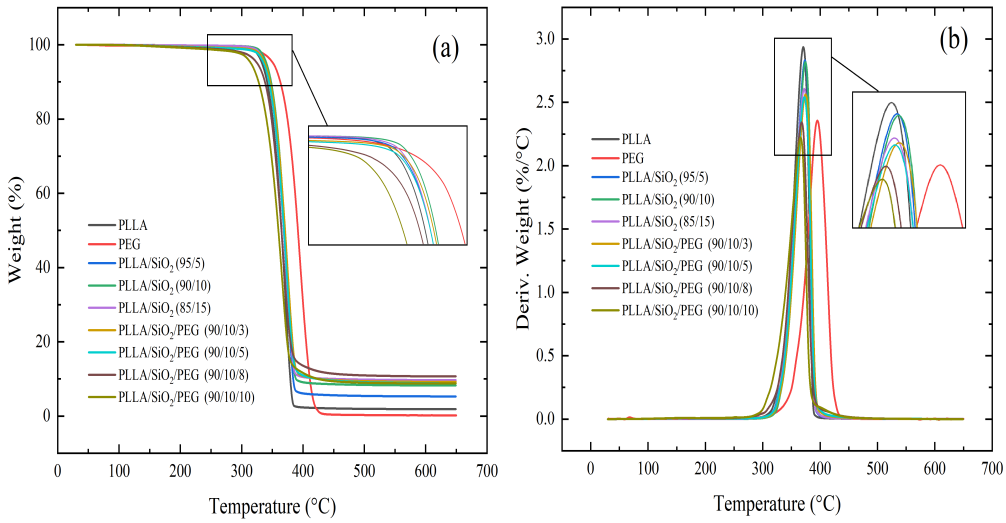

Figure 8. Thermogravimetric analysis of PLLA, PEG, PLLA/SiO_2, and PLLA/SiO_2/PEG: (**a**) weight curves (TGA) and (**b**) their derivatives (DTA).

Table 8. TGA results of PLLA, PLLA/SiO_2, and PLLA/SiO_2/PEG (10 °C/min in N_2).

Sample	T_{onset} (°C)	T_{endset} (°C)	$T_{degradation}$ (°C)	Total Loss (%)
PLLA	9.67	96.9	36.0	98.8
PLLA/SiO_2 (95/5)	8.36	83.8	31.1	94.7
PLLA/SiO_2 (90/10)	5.75	57.7	21.4	91.7
PLLA/SiO_2 (85/15)	8.03	80.5	29.9	91.2
PLLA/SiO_2/PEG (90/10/3)	5.18	51.9	19.2	90.8
PLLA/SiO_2/PEG (90/10/5)	6.17	61.9	23.0	91.1
PLLA/SiO_2/PEG (90/10/8)	4.54	45.5	16.9	90.3
PLLA/SiO_2/PEG (90/10/10)	5.18	51.9	19.2	89.3

Using the Friedman method, the calculated results of kinetic parameters for the thermal degradation of all composites are given in Table 9. The values were obtained by plotting ln(dα/dt) as a function of $(1/T)$ with the slope being (E_a/R). The order of the reaction (n) for PLLA is 1.3, whereas E_a is 201.6 kJ/mol, which is higher than the one found in the literature of 161 kJ/mol [68,90]. The difference can be explained as follows. Friedman's method is well known for being very sensitive to experimental noise and numerically unstable due to the use of instantaneous rate values [91]. However, E_a for the composites increases with SiO_2 content resulting in substantially higher thermal stability. Furthermore, PEG composites have lower E_a values, indicating lower thermal stability as observed from the TGA results (Figure 8 and Table 9).

Table 9. Kinetic parameters (TGA) of PLLA, PLLA/SiO_2, and PLLA/SiO_2/PEG (10 °C/min).

Sample	E_a (kJ/mol)	n	Ln(A)	R^2
PLLA	201.6	1.3	39.18	0.992
PLLA/SiO_2 (95/5)	212.2	1.7	41.02	0.993
PLLA/SiO_2 (90/10)	247.9	1.1	47.83	0.995
PLLA/SiO_2 (85/15)	218.7	1.3	42.35	0.990
PLLA/SiO_2/PEG (90/10/3)	241.4	1.2	46.56	0.992
PLLA/SiO_2/PEG (90/10/5)	227.8	1.2	44.07	0.994
PLLA/SiO_2/PEG (90/10/8)	214.7	1.0	41.76	0.993
PLLA/SiO_2/PEG (90/10/10)	156.4	0.9	30.68	0.994

3.4. Melt Rheology

The rheological properties are important because adding solid particles to a polymer can change its viscoelastic behavior [92]. Figure 9 presents the rheological properties of PLLA and the composites at their processing temperature (190 °C). Figure 9a shows that the complex viscosity (η^*) decreases with angular frequency, which is a typical shear-thinning behavior for most thermoplastics in the melting state. However, η^* increases with increasing silica content which can be associated with the flow line disruption and restriction of polymer chain mobility by the presence of rigid particles [92]. As a result, the storage modulus (G′) and loss modulus (G″) increase progressively with increasing frequency and filler content in agreement with linear viscoelasticity theory [93]. Figure 9d shows that PLLA/SiO_2 have higher damping factors (tan δ) than the neat PLLA because of restricted chain mobility, especially at lower frequencies. Finally, increasing the PEG concentration significantly decreased the viscosity [94]. The PEG molecules, acting as a plasticizer, produced some disentanglement and improved the segmental mobility of PLLA chains [87]. Consequently, the η^*, G′, and G″ trends indicate that the materials became more viscous than elastic [95]. The (tan δ) curves seem to be shifted to higher frequencies indicating a faster melt response (lower characteristic times).

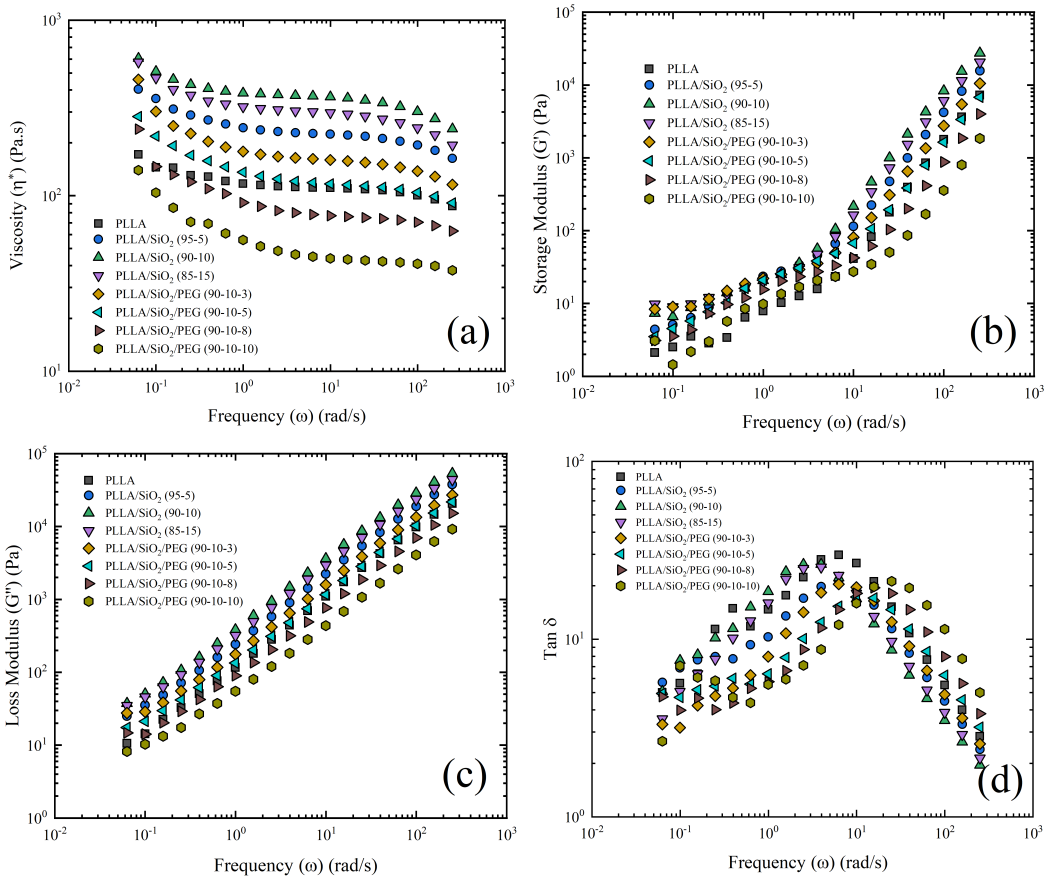

Figure 9. Rheological properties as a function of frequency: (**a**) complex viscosity, (**b**) storage modulus, (**c**) loss modulus, and (**d**) damping factor (tan δ) for PLLA, PLLA/SiO_2, and PLLA/SiO_2/PEG (190 °C).

3.5. Tensile Properties

The tensile properties of all the samples are presented in Figure 10. The incorporation of SiO_2 in PLLA significantly decreases the tensile strength and elongation at the break of the composites with increasing silica content. Since there is no chemical bonding between the PLLA and SiO_2 particles, the composites' integrity depends only on physical interactions between the filler and the matrix. Limited interfacial stress transfer is expected,

leading to lower tensile strength [96]. Nevertheless, Young's modulus increased by 26% for 10 wt.% SiO_2 due to the reinforcing effect of rigid particles [97,98], but did not further improve at high content due to possible particle–particle contact (defects). Previous works showed that these defects occurred at higher particle concentrations due to particle size and agglomeration effects within the polymer matrix. Smaller particles have a larger total surface area for a given particle content, implying that the rupture tension increases as the surface area of the packed particles grows due to a more efficient stress transfer mechanism [99–102]. In this work, amorphous SiO_2 particles with an average size of 10–40 µm were used, hindering an effective stress transfer and decreasing Young's modulus, as discussed above. In addition, several investigations showed that decreasing elastic modulus is related to the cooling rate: the degree of crystallinity increases when the polymer is slowly cooled down [103–105].

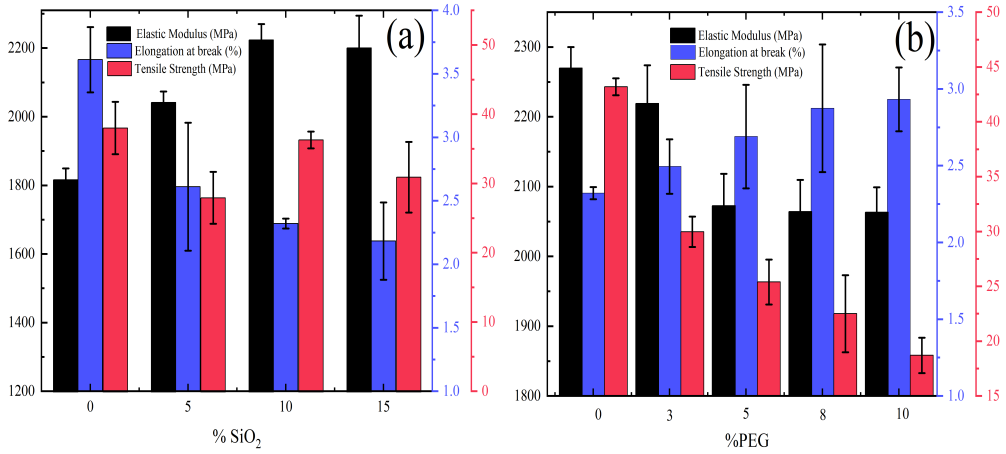

Figure 10. Mechanical properties (elastic modulus, tensile strength, and elongation at break) of: (**a**) PLLA/SiO_2 and (**b**) PLLA/SiO_2/PEG composites.

In order to compensate for the brittleness introduced by SiO_2 addition, PEG was added as a plasticizer. As an effective PLLA plasticizer, PEG promotes PLLA segment mobility and elongation [106]. Figure 10b shows that increasing the PEG content into PLLA/SiO_2 (90/10) decreases Young's modulus while increasing the elongation at break. These results confirm the plasticizing effect of PEG, increasing the homogeneous dispersion of SiO_2 in the matrix (Figure 2). Nevertheless, the composites have better elasticity/ductility (lower stiffness) [17]. As reported in Figure 3 and Table 2, the crystallinity increases with PEG content which might also contribute to a final balance between rigidity and deformation. Plasticizers also reduce the T_g (Figure 3 and Table 2) allowing more intramolecular interactions and mobility between the polymer and plasticizer molecules [13].

The fracture surfaces of the tensile specimens were investigated by SEM, where significant differences can be seen compared to Figure 2. Figure 11a does not show any necking because it is rigid and produces a brittle failure (PLLA) [72]. Figure 11b–d shows a poor distribution of SiO_2 and a similar brittle failure suggesting that the matrix and filler do not interact. In these samples, the presence of the neck is not observed, but the break is similar to that of neat PLLA. This trend also explains why most mechanical properties decreased with increasing SiO_2 concentration. Nevertheless, adding a plasticizer (PEG) to the PLLA matrix improved the filler–matrix interaction. PEG promotes SiO_2 dispersion in PLLA because it acts as a lubricant for the PLLA chains (Figure 11e–h). In the composites with PEG, the formation of a neck was present for the samples with high PEG content (above 8%). Furthermore, the number of fibrils and their contact with SiO_2 increased at higher PEG concentrations, improving matrix–particle interactions. As a result, the thermal (Table 5) and mechanical (Figure 10) properties were improved.

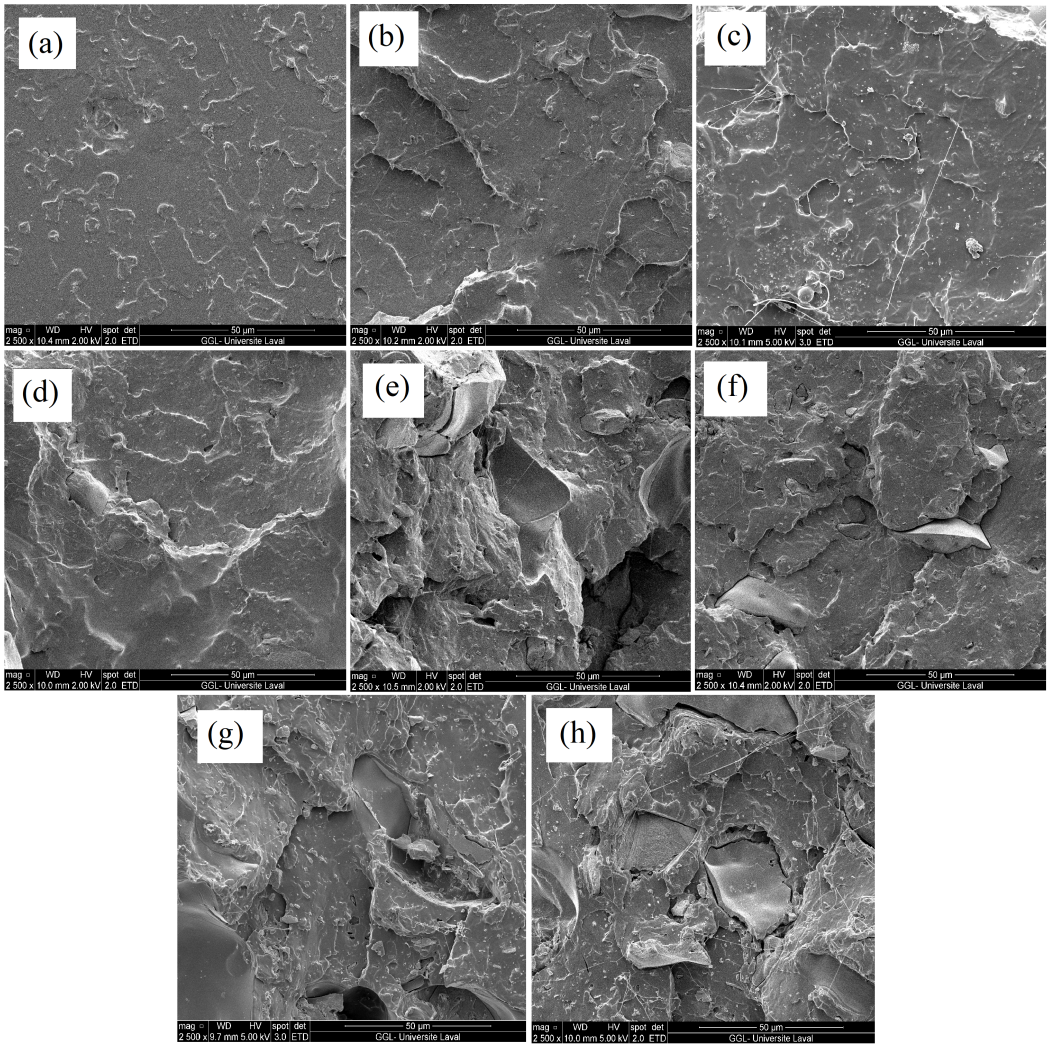

Figure 11. SEM micrograph of the tensile test rupture surface of: (**a**) neat PLLA, (**b**) PLLA/SiO_2 (95/5), (**c**) PLLA/SiO_2 (90/10), (**d**) PLLA/SiO_2 (85/15), (**e**) PLLA/SiO_2/PEG (90/10/3), (**f**) PLLA/SiO_2/PEG (90/10/5), (**g**) PLLA/SiO_2/PEG (90/10/8), (**h**) PLLA/SiO_2/PEG (90/10/10).

3.6. X-ray Diffraction Analysis

X-ray diffraction patterns were carried out to determine the crystal structures in the PLLA composites. The samples were thermally treated to enhance their crystallinity content and to provide more accurate XRD patterns for the relevant analyses. Figure 12 presents the XRD patterns of all composites, which contain four distinctive diffraction peaks. These peaks are characteristic of the α-crystalline phase of PLLA. For PLLA/SiO_2 composites, there is no significant change in the shape and position of these peaks. In contrast, when 3 wt.% PEG was incorporated, the diffraction peaks became shape-formed and shifted to higher 2θ positions. The peak at 2θ = 16.3° represents the α'-crystalline phase with lower packing density due to incomplete crystallization [107]. The intensity of this peak at 10 wt.% PEG increased and was shifted to 2θ= 16.6°. In addition, three more peaks appeared and were shifted to higher positions: at 2θ = 14.7, 18.7, and 22.1°, corresponding to the lattice planes (200)/(100), (203), and (015), respectively. Table 10 reports the crystallinity degree determined using XRD patterns to compare with DSC results. XRD values are found to be much higher than for DSC because of their different thermal treatment (history). It is also observed that increasing the PEG content leads to higher crystallinity. As a result, it is concluded that PEG efficiently promotes the mobility of PLLA chains, even when SiO_2 particles are present.

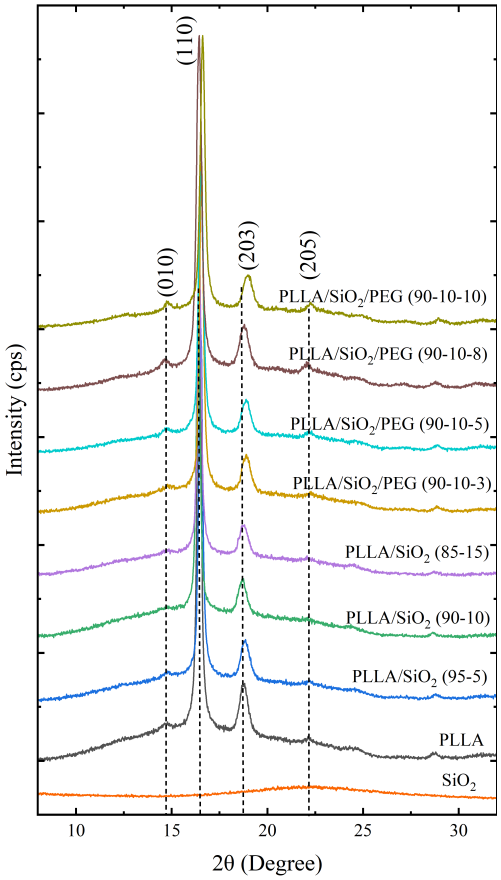

Figure 12. XRD patterns of PLLA, PLLA/SiO_2, and PLLA/SiO_2/PEG.

Table 10. Crystallinity (Xc) of PLLA, PLLA/SiO_2, and PLLA/SiO_2/PEG obtained from XRD patterns and DSC.

Sample	XRD (Xc%)	DSC (Xc%)
PLLA	33.5	3.4
PLLA/SiO_2 (95/5)	30.9	2.3
PLLA/SiO_2 (90/10)	30.9	4.6
PLLA/SiO_2 (85/15)	29.4	4.7
PLLA/SiO_2/PEG (90/10/3)	30.9	2.3
PLLA/SiO_2/PEG (90/10/5)	31.0	3.8
PLLA/SiO_2/PEG (90/10/8)	33.6	6.4
PLLA/SiO_2/PEG (90/10/10)	30.6	6.5

3.7. Gas Permeation Measurements

One of the reasons for conducting this research was industrial interest in polymeric gas-separating membranes [108]. The use of fillers to improve the gas permeability of PLLA has been well documented [103,109,110]. In our study, the effect of silica on the permeability of PLLA and its composites was investigated, and Table 11 presents the results obtained by the variable pressure method at 35 °C and 40 psi. In general, the composites' gas permeability (O_2, N_2, CO_2, and CH_4) decreases as crystallinity increases, which is related to the lower amount of amorphous zones in the polymer. There is also less free volume [110]. PLLA/SiO2 with 15 wt.% had improved barrier properties decreasing the permeability for O_2 (−30%) and CO_2 (−33%), whereas for 10 wt.%, an increase in permeability was observed for H_2 (+81%) and CH_4 (+25%). This trend can be explained by some micropores and defects being sealed by SiO_2, showing a selective character for those gases. There are also possible interactions between the different gases and the polymer particles. According to the values obtained for selectivity, higher values were achieved with 10 wt.% of silica.

However, these values can be improved by changing some parameters, such as temperature and/or pressure [103].

Table 11. Permeability of O_2, CO_2, H_2, and CH_4 in PLLA, PLLA/SiO_2, and PLLA/SiO_2/PEG.

Sample	Permeability (cm^3 cm cm^{-2} s^{-1} $cmHg^{-1}$)				Selectivity (-)			
	O_2	CO_2	H_2	CH_4	H_2/O_2	CH_4/CO_2	H_2/CO_2	H_2/CH_4
PLLA	9.36	7.49	5.56	6.53	1.68	1.15	1.35	1.17
PLLA/SiO_2 (95/5)	7.30	6.98	9.04	9.07	1.24	1.30	1.30	1.00
PLLA/SiO_2 (90/10)	6.34	6.73	10.1	8.17	1.59	1.21	1.50	1.24
PLLA/SiO_2 (85/15)	6.46	4.98	7.26	5.61	1.12	1.13	1.46	1.29
PLLA/SiO_2/PEG (90/10/3)	4.45	4.69	5.84	5.60	1.31	1.19	1.25	1.04
PLLA/SiO_2/PEG (90/10/5)	4.41	4.60	6.02	4.01	1.37	1.15	1.31	1.50
PLLA/SiO_2/PEG (90/10/8)	4.80	4.98	6.10	6.11	1.27	1.23	1.22	1.00
PLLA/SiO_2/PEG (90/10/10)	3.56	3.76	4.02	5.48	1.13	1.46	1.07	1.36

On the other hand, the results for PLLA/SiO_2/PEG composites show a decrease in permeability for all the gases compared with neat PLLA. The variation can be important: up to 62% for O_2. As reported in Figures 2 and 11, increasing the PEG content increased the dispersion of SiO_2 particles into the polymeric matrix, leading to fewer defects. As a result, a more difficult mass transfer of the molecules throughout the composites is produced, and the gas molecules have more resistance to permeate the material [97]. Although the permeability significantly decreases for all gases, there is still a difference between O_2 and CO_2 in comparison with H_2 and CH_4. These results indicate that different formulations can be used depending on the final application.

Battegazzore et al. [48] observed that the presence of extracted silica (5, 10, 20, and 30 wt.%) in PLA resulted in significant increases in Young's modulus (+32%) and a slight decrease in the oxygen permeability (−19%). In this work, Young's modulus increased (+26%), whereas the permeability to oxygen decreased (−62%) creating films with selective characteristics. In addition, an analysis with CO_2 (−50%), H_2 (−27%), and CH_4 (−16%) gas was performed. Aydin and Geyikçi [47] reported that PLA/PEG/SiO_2 films had improved thermal stability (+23%) with increasing silica concentration. In this work, the thermal stability was improved by 23%. A complete study of the properties of PLLA was carried out and the isothermal analysis allowed us to explain the physical behavior of the composites from the perspective of polymer crystallization. The rheological analysis also allowed us to understand the viscoelastic behavior of this composite for its possible application to a final product. In the same way, a study was also carried out on the crystalline structure with XPS of the material to know the interactions between PLLA, PEG, and SiO_2, obtaining conclusive results related to its thermal properties.

4. Final Remarks and Future Works

Green and renewable resources are in more demand than ever. For example, blends and composites made from poly(lactic) acid have found significant use in eco-friendly packaging. Although these are gaining in popularity as alternatives to current petroleum-based plastics, their extensive use is now constrained by their high cost and low level of manufacture (more difficult processing) [111,112]. Due to its biodegradable nature, PLA can be used to create loose-fill packaging, compost bags, food packaging, and disposable dinnerware. Nevertheless, more than brittleness and other properties, such as low heat stability, average gas barrier characteristics, and moderate solvent resistance, it must be improved for food packaging applications [112,113]. Fibers or filler addition is one method for enhancing PLA's mechanical and thermal properties. Bio-composites are important for several applications, as diverse renewable and non-renewable elements are used to create bio-composites. This work investigated SiO_2 from rice husk as a filler for PLLA and PEG as a plasticizer for its application in food packaging. The rice husk was selected because waste can generate a circular economy. The market for PLLA/SiO_2 composites will continue

to expand. Here are some relatively new areas we believe future research on PLA/silica composites should concentrate on:

- With several new applications in various disciplines, including the aerospace, energy, and chemical industries, packaging is anticipated to be available shortly. However, the dispersion of silica particles in the PLLA matrix should be improved.
- Barrier properties are extremely important in food packaging. Future work should investigate the permeability to water vapor, oxygen, and carbon dioxide to obtain good candidates for bio-packaging.
- Plasticizers are used to improve the mechanical properties of PLLA and obtain similar properties to those of synthetic polymers. The improvement and development of new components to obtain these properties will be a promising area of research.
- Reduction in production costs for PLLA will be a trend that will continue to be studied in future work since the production of this biopolymer will increase and routes developed to reduce production costs.

5. Conclusions

PLLA/SiO_2 and PLLA/SiO_2/PEG composites were prepared using melt extrusion for compounding and compression molding. A series of analyses were performed to relate the performances of the composites depending on their composition and morphology. The results of the current research work led to the following observations:

1. Morphological analyses showed no agglomeration and good interaction between the particles and the polymeric matrix. Due to the high miscibility between both polymers and the high amount of hydroxyl groups present in SiO_2, adding PEG to the composite increased the SiO_2 distribution, leading to more homogeneous samples and smoother surfaces after breakup.
2. Non-isothermal analysis showed that incorporating SiO_2 at higher concentrations (10–15 wt.%) increased T_g and T_{cc} hindering PLLA crystallization as confirmed by XRD analysis. In contrast, the addition of PEG to the PLLA/SiO_2 (90/10) composite showed lower T_g and T_{cc}, mainly due to the plasticizing effect of PEG increasing chain mobility.
3. The Avrami and Lauritzen–Hoffman parameters confirmed that silica particles make the crystallization of PLLA more difficult due to an impeding effect, especially at higher concentrations, whereas for composites with PEG, lower energy is required for the chain folding process.
4. The thermal stability of the composites with SiO_2 increased because of the presence of highly stable particles (SiO_2) up to 23%.
5. SiO_2 addition also increased the viscosity due to the disruption of the flow lines and more restrictions on the polymer chains' mobility. However, for PEG, the values of (η^*, G′, and G″) decreased improving fluidity.
6. Incorporating 10 wt.% of SiO_2 to PLLA, the tensile modulus increase (26%), while slightly decreasing (2.4%) the tensile strength. Nevertheless, composite with higher PEG content (10 wt.%) exhibited the optimum elongation at break (26%) contributing to a final balance between rigidity and deformation.
7. According to gas permeation measurements, PLLA with 5 and 10 wt.% SiO_2 exhibits an improvement in the PLLA's barrier properties for O_2 and CO_2, while increasing the permeability for H_2 and CH_4. Due to the saturation of SiO_2 and Si-O bonds on the surface of the polymeric matrix combined with increased crystallinity. However, the permeability for all gases decreased up to 62% for O_2 with increasing PEG content since better SiO_2 particle distribution was obtained (fewer defects), reducing the free volume and generating more resistance for the molecules to permeate (lower mass transfer) through the composites.

Supplementary Materials: The following supporting information can be downloaded at: https://www.mdpi.com/article/10.3390/jcs7040150/s1, Figure S1: DSC thermograms of (a) first heating and (b) cooling step for PLLA, PLLA/SiO_2 and PLLA/SiO_2/PEG composites. Table S1: Avrami fitting parameters (n, K, and $\tau_{theo}^{1/2}$) and their correlation coefficient (R^2). The experimental value of $\tau^{1/2}$ is given for comparison purposes. The conversion range used was the same in each case (5–20%). Figure S2: Variation of $1 - V_c$ (volumetric relative amorphous content) as a function of $\log(t - t_0)$. The lines represent fitting to the Avrami model (Equation (3)) with the parameters of Table 6. The crystallization temperatures were 97, 100, and 107 °C for PLLA, PLLA/SiO_2 (95-5), and PLLA/SiO_2/PEG (90-10-3), respectively. Figure S3: Variation of the enthalpy of crystallization (ΔH_c) as a function of time (t) for PLLA, PLLA/SiO_2 (95-5), and PLLA/SiO_2/PEG (90-10-3). Figure S4: Experimental DSC isotherms and simulated DSC curves by the Avrami equation for PLLA, PLLA/SiO_2 (95-5), and PLLA/SiO_2/PEG (90-10-3). The crystallization temperatures were 97, 100, and 107 °C for PLLA, PLLA/SiO_2 (95-5), and PLLA/SiO_2/PEG (90-10-3), respectively. Figure S5: Plots of $\ln(1/t_{1/2}) + U(^*)/R(T_c - T_\infty)$ as a function of $(1/T_c \Delta T f)$ for PLLA, PLLA/SiO_2 (95-5), PLLA/SiO_2 (90-10), and PLLA/SiO_2 (85-15). Figure S6: Plots of $\ln(1/t_{1/2}) + U(^*)/R(T_c - T_\infty)$ as a function of $(1/T_c \Delta T f)$ for PLLA/SiO_2/PEG composites.

Author Contributions: Conceptualization, J.M. and R.M.M.; methodology, J.M.; validation, R.M.M., A.S.-M. and D.R.; investigation, J.M.; resources, D.R.; data curation, J.M.; writing—original draft preparation, J.M.; visualization, J.M.; supervision, D.R., R.M.M. and A.S.-M.; funding acquisition, D.R. and A.S.-M. All authors have read and agreed to the published version of the manuscript.

Funding: Award by Global Affairs Canada for the scholarship through the 2021–2022 Emerging Leaders in the Americas Program (ELAP).

Data Availability Statement: The data are available upon request to the authors.

Acknowledgments: The authors acknowledge Edward Avila for the X-ray diffraction patterns used in this study.

Conflicts of Interest: The authors declare no conflict of interest.

References

1. Madhavan Nampoothiri, K.; Nair, N.R.; John, R.P. An overview of the recent developments in polylactide (PLA) research. *Bioresour. Technol.* **2010**, *101*, 8493–8501. [CrossRef] [PubMed]
2. Lunt, J. Large-scale production, properties and commercial applications of poly lactic acid polymers. *Polym. Degrad. Stab.* **1998**, *59*, 145–152. [CrossRef]
3. Auras, R.; Harte, B.; Selke, S. An overview of polylactides as packaging materials. *Macromol. Biosci.* **2004**, *4*, 835–864. [CrossRef]
4. He, Y.; Fan, Z.; Hu, Y.; Wu, T.; Wei, J.; Li, S. DSC analysis of isothermal melt-crystallization, glass transition and melting behavior of poly(l-lactide) with different molecular weights. *Eur. Polym. J.* **2007**, *43*, 4431–4439. [CrossRef]
5. Drumright, R.E.; Gruber, P.R.; Henton, D.E. Polylactic acid technology. *Adv. Mater.* **2000**, *12*, 1841–1846. [CrossRef]
6. Garlotta, D. A literature review of poly(lactic acid). *J. Polym. Environ.* **2001**, *9*, 63–84. [CrossRef]
7. Stefaniak, K.; Masek, A. Green copolymers based on poly(Lactic acid)—Short review. *Materials* **2021**, *14*, 5254. [CrossRef] [PubMed]
8. Lai, W.C.; Liau, W.B.; Lin, T.T. The effect of end groups of PEG on the crystallization behaviors of binary crystalline polymer blends PEG/PLLA. *Polymer* **2004**, *45*, 3073–3080. [CrossRef]
9. Wypych, G. PLA poly(lactic acid). In *Handbook of Polymers*; Elsevier: Amsterdam, The Netherlands, 2012; pp. 436–440. [CrossRef]
10. Farah, S.; Anderson, D.G.; Langer, R. Physical and mechanical properties of PLA, and their functions in widespread applications—A comprehensive review. *Adv. Drug. Dev. Rev.* **2016**, *107*, 367–392. [CrossRef]
11. Buwalda, S.J.; Dijkstra, P.J.; Feijen, J. Poly(ethylene glycol)-poly(L-lactide) star block copolymer hydrogels crosslinked by metal-ligand coordination. *J. Polym. Sci. Part A Polym. Chem.* **2012**, *50*, 1783–1791. [CrossRef]
12. Hasanuddin, N.I.; Mokhtar, W.N.A.W.; Othaman, R.; Anuar, F.H. Poly(lactic acid)-poly(ethylene glycol)/Magnesium Silicate Membrane for Methylene Blue Removal: Adsorption Behavior, Mechanism, Ionic Strength and Reusability Studies. *Membranes* **2022**, *12*, 198. [CrossRef] [PubMed]
13. Long, H.; Wu, Z.; Dong, Q.; Shen, Y.; Zhou, W.; Luo, Y.; Zhang, C.; Dong, X. Effect of polyethylene glycol on mechanical properties of bamboo fiber-reinforced polylactic acid composites. *J. Appl. Polym. Sci.* **2019**, *136*, 3–10. [CrossRef]
14. Prapruddivongs, C.; Apichartsitporn, M.; Wongpreedee, T. Effect of Commercial SiO_2 and SiO_2 from rice husk ash loading on biodegradation of Poly (lactic acid) and crosslinked Poly (lactic acid). *IOP Conf. Ser. Mater. Sci. Eng.* **2017**, *244*, 012007. [CrossRef]
15. Athanasoulia, I.G.; Tarantili, P.A. Preparation and characterization of polyethylene glycol/poly(L-lactic acid) blends. *Pure Appl. Chem.* **2017**, *89*, 141–152. [CrossRef]

16. Zubir, N.H.M.; Sam, S.T.; Zulkepli, N.N.; Omar, M.F. The effect of rice straw particulate loading and polyethylene glycol as plasticizer on the properties of polylactic acid/polyhydroxybutyrate-valerate blends. *Polym. Bull.* **2018**, *75*, 61–76. [CrossRef]
17. Rahman, M.A.; De Santis, D.; Spagnoli, G.; Ramorino, G.; Penco, M.; Phuong, V.T.; Lazzeri, A. Biocomposites based on lignin and plasticized poly(L -lactic acid). *J. Appl. Polym. Sci.* **2013**, *129*, 202–214. [CrossRef]
18. Zhang, Y.; Li, T.; Jin, Y.; Bao, L.; Feng, L.; Lai, C.; Wei, K. Thermo-regulated thermoplastic sugarcane bagasse-based biocomposite via solvent-free extrusion for energy-saving smart home. *Chem. Eng. J.* **2023**, *458*, 141437. [CrossRef]
19. Li, T.; Zhang, Y.; Jin, Y.; Bao, L.; Dong, L.; Zheng, Y.; Xia, J.; Jiang, L.; Kang, Y.; Wang, J. Thermoplastic and biodegradable sugarcane lignin-based biocomposites prepared via a wholly solvent-free method. *J. Clean. Prod.* **2023**, *386*, 135834. [CrossRef]
20. Mahmoud, M.; Zaghloul, Y.; Yousry, M.; Zaghloul, M.; Mahmoud, M.; Zaghloul, Y. Experimental and modeling analysis of mechanical-electrical behaviors of polypropylene composites fi lled with graphite and MWCNT fi llers. *Polym. Test.* **2017**, *63*, 467–474. [CrossRef]
21. Mahmoud, M.; Zaghloul, Y.; Mohamed, Y.S. Fatigue and tensile behaviors of fiber-reinforced thermosetting composites embedded with nanoparticles. *J. Compos. Mater.* **2019**, *53*, 709–718. [CrossRef]
22. Yousry, M.; Zaghloul, M.; Mahmoud, M.; Zaghloul, Y.; Mahmoud, M.; Zaghloul, Y. Physical analysis and statistical investigation of tensile and fatigue behaviors of glass fi ber-reinforced polyester via novel fi bers arrangement. *J. Compos. Mater.* **2023**, *57*, 147–166. [CrossRef]
23. Mahmoud, M.; Zaghloul, Y.; Mahmoud, M.; Zaghloul, Y. Influence of flame retardant magnesium hydroxide on the mechanical properties of high density polyethylene composites. *J. Reinf. Plast. Compos.* **2017**, *36*, 1802–1816. [CrossRef]
24. Mahmoud, M.; Mahmoud, Y. Mechanical properties of linear low-density polyethylene fi re-retarded with melamine polyphosphate. *J. Appl. Polym. Sci.* **2018**, *46770*, 1–12. [CrossRef]
25. Yousry, M.; Zaghloul, M.; Mahmoud, M.; Zaghloul, Y.; Mahmoud, M.; Zaghloul, Y. Developments in polyester composite materials—An in-depth review on natural fibres and nano fillers. *Compos. Struct.* **2021**, *278*, 114698. [CrossRef]
26. Fuseini, M.; Mahmoud, M.; Zaghloul, Y. Investigation of Electrophoretic Deposition of PANI Nano fibers as a Manufacturing Technology for corrosion protection. *Prog. Org. Coatings* **2022**, *171*, 107015. [CrossRef]
27. Masnar, A.; Coorey, R. Application of sago pith waste and nanosilica from rice husk ash as hybrid bio-nanofiller composite for food plastic packaging. *Bio. Food. Plast. Pack.* **2017**, *6*, 618–631. [CrossRef]
28. Vedernikov, A.; Safonov, A.; Tucci, F.; Carlone, P.; Akhatov, I. Analysis of spring-in deformation in L-shaped profiles pultruded at different pulling speeds: Mathematical simulation and experimental results. In Proceedings of the ESAFORM: 24th International Conference on Material Forming, Liège, Belgium, 14–16 April 2021. [CrossRef]
29. Tucci, F.; Vedernikov, A. Design criteria for Pultruded Structural Elements. *J. Compos. Mater.* **2021**, *3*, 51–68. [CrossRef]
30. Minchenkov, K.; Vedernikov, A.; Kuzminova, Y.; Gusev, S.; Sulimov, A.; Gulyaev, A.; Kreslavskaya, A.; Prosyanoy, I.; Xian, G.; Akhatov, I.; et al. Effects of the quality of pre-consolidated materials on the mechanical properties and morphology of Thermoplastic pultruded flat laminates. *Compos. Commun.* **2022**, *35*, 101281. [CrossRef]
31. Zhou, P.; Li, C.; Bai, Y.; Dong, S.; Xian, G.; Vedernikov, A.; Akhatov, I.; Safonov, A.; Yue, Q. Durability study on the interlaminar shear behavior of glass-fibre reinforced polypropylene (GFRPP) bars for marine applications. *Constr. Build. Mater.* **2022**, *349*, 128694. [CrossRef]
32. Madenci, E.; Özkılıç, Y.O.; Aksoylu, C.; Safonov, A. The effects of eccentric web openings on the compressive performance of pultruded GFRP boxes wrapped with GFRP and CFRP sheets. *Polymers* **2022**, *14*, 4567. [CrossRef]
33. Ozkilic, Y.O.; Gemi, L.; Madenci, E.; Aksoylu, C.; Kalkan, I. Effect of the GFRP wrapping on the shear and bending Behavior of RC beams with GFRP encasement. *Steel. Compos. Struct.* **2022**, *45*, 193–204. [CrossRef]
34. Desai, N.P.; Hubbell, J.A. Solution technique to incorporate polyethylene oxide and other water-soluble polymers into surfaces of polymeric biomaterials. *Biomaterials* **1991**, *12*, 144–153. [CrossRef] [PubMed]
35. Jacobsen, S.; Fritz, H. Plasticizing polylactide—the effect of different plasticizers on the mechanical properties. *Polym. Eng. Sci.* **1999**, *39*, 1303–1310. [CrossRef]
36. Sheth, M.; Kumar, R.A.; Dave, V. Biodegradable Polymer Blends of poly(lactic acid) and poly(ethylene glycol) PL. *J. Appl. Polym. Sci.* **2008**, *66*, 1495–1505. [CrossRef]
37. Battegazzore, D.; Noori, A.; Frache, A. Natural wastes as particle filler for poly(lactic acid)-based composites. *J. Compos. Mater.* **2019**, *53*, 783–797. [CrossRef]
38. Lohar, D.V.; Nikalje, A.M.; Damle, P.G. Development and testing of hybrid green polymer composite (HGPC) filaments of PLA reinforced with waste bio fillers. *Mater. Today Proc.* **2022**, *62*, 818–824. [CrossRef]
39. Pavon, C.; Aldas, M.; Motoc, D.L.; Ferrandiz, S.; Juan, L. Behavior of 3D-Printed PLA Reinforced with $CaCO_3$ Fillers from Natural Resources. *Polymers* **2022**, *14*, 2646. [CrossRef]
40. Imam, M.A.; Jeelani, S.; Rangari, V.K. Thermal decomposition and mechanical characterization of poly (lactic acid) and potato starch blend reinforced with biowaste SiO_2. *J. Compos. Mater.* **2019**, *53*, 2315–2334. [CrossRef]
41. Kane, S.; Ryan, C. Biochar from food waste as a sustainable replacement for carbon black in upcycled or compostable composites. *JCOMC* **2022**, *8*, 100274. [CrossRef]
42. Chougan, M.; Ghaffar, S.H.; Al-Kheetan, M.J.; Gecevicius, M. Wheat straw pre-treatments using eco-friendly strategies for enhancing the tensile properties of bio-based polylactic acid composites. *Ind. Crop. Prod.* **2020**, *155*, 112836. [CrossRef]

43. Yiga, V.A.; Pagel, S.; Lubwama, M.; Epple, S.; Olupot, P.W.; Bonten, C. Development of fiber-reinforced polypropylene with NaOH pretreated rice and coffee husks as fillers: Mechanical and thermal properties. *J. Thermoplast. Compos. Mater.* **2020**, *33*, 1269–1291. [CrossRef]
44. Yalçin, N.; Sevinç, V. Studies on silica obtained from rice husk. *Ceram. Int.* **2001**, *27*, 219–224. [CrossRef]
45. Hernández-Olivares, F.; Elizabeth Medina-Alvarado, R.; Burneo-Valdivieso, X.E.; Rodrigo Zúñiga-Suárez, A. Short sugarcane bagasse fibers cementitious composites for building construction. *Constr. Build. Mater.* **2020**, *247*, 8–10. [CrossRef]
46. Ahmed, W.; Siraj, S.; Al-Marzouqi, A.H. 3d printing pla waste to produce ceramic based particulate reinforced composite using abundant silica-sand: Mechanical properties characterization. *Polymers* **2020**, *12*, 2579. [CrossRef] [PubMed]
47. Aydin, B.; Geyikçi, F. Effect of Silica Obtained From Rice Husk on the Structural and Thermal Properties of Polylactic Acid/Polyethylene Glycol Films. *Mugla J. Sci. Technol.* **2019**, *5*, 91–96. [CrossRef]
48. Battegazzore, D.; Bocchini, S.; Alongi, J.; Frache, A. Rice husk as bio-source of silica: Preparation and characterization of PLA-silica bio-composites. *RSC Adv.* **2014**, *4*, 54703–54712. [CrossRef]
49. Díez-Rodríguez, T.M.; Blázquez-Blázquez, E.; Martínez, J.C.; Pérez, E.; Cerrada, M.L. Composites of a PLA with SBA-15 mesoporous silica: Polymorphism and properties after isothermal cold crystallization. *Polymer* **2022**, *241*, 124515. [CrossRef]
50. Opaprakasit, P.; Boonpa, S.; Jaikaew, N.; Petchsuk, A.; Tangboriboonrat, P. Preparation of surface-modified silica particles from rice husk ash and its composites with degradable polylactic acid. *Macromol. Symp.* **2015**, *354*, 48–54. [CrossRef]
51. Soltani, N.; Bahrami, A.; Pech-Canul, M.I.; González, L.A. Review on the physicochemical treatments of rice husk for production of advanced materials. *Chem. Eng. J.* **2015**, *264*, 899–935. [CrossRef]
52. Yiga, V. A.; Lubwama, M.; Olupot, P.W. Thermal stability of unmodified and alkali modified rice husks for flame retardant fiber reinforced PLA composites. *J. Therm. Anal. Calorim.* **2022**, *147*, 11049–11075. [CrossRef]
53. Le Guen, M.J.; Hill, S.; Smith, D.; Theobald, B.; Gaugler, E.; Barakat, A.; Mayer-Laigle, C. Influence of Rice Husk and Wood Biomass Properties on the Manufacture of Filaments for Fused Deposition Modeling. *Front. Chem.* **2019**, *7*, 15–20. [CrossRef] [PubMed]
54. Tipachan, C.; Gupta, R.K.; Agarwal, S.; Kajorncheappunngam, S. Flame retardant properties and thermal stability of polylactic acid filled with layered double hydroxide and rice husk ash silica. *J. Polym. Environ.* **2020**, *28*, 948–961. [CrossRef]
55. Saeidlou, S.; Huneault, M.A.; Li, H.; Park, C.B. Poly(lactic acid) crystallization. *Prog. Polym. Sci.* **2012**, *37*, 1657–1677. [CrossRef]
56. NatureWorks. *Ingeo Biopolymer 4043D Technical Data Sheet*; Technical Report 4; NatureWorks: Minnetonka, MN, USA, 2015.
57. Barkhad, M.S.; Abu-jdayil, B.; Mourad, A.H.I.; Iqbal, M.Z. Thermal Insulation and Mechanical Properties of Polylactic Acid (PLA) at Different Processing Conditions. *Polymers* **2020**, *12*, 2091. [CrossRef]
58. Yu, W.; Wang, X.; Ferraris, E.; Zhang, J. Melt crystallization of PLA/Talc in fused fi lament fabrication. *Mater. Des.* **2019**, *182*, 108013. [CrossRef]
59. Yussuf, A.A.; Massoumi, I.; Hassan, A. Comparison of polylactic Acid/Kenaf and polylactic Acid/Rise husk composites: The influence of the natural fibers on the mechanical, thermal and biodegradability properties. *J. Polym. Environ.* **2010**, *18*, 422–429. [CrossRef]
60. Jia, S.; Yu, D.; Zhu, Y.; Wang, Z.; Chen, L.; Fu, L. Morphology, Crystallization and Thermal Behaviors of PLA-Based Composites: Wonderful Effects of Hybrid GO/PEG via Dynamic Impregnating. *Polymers* **2017**, *9*, 528. [CrossRef]
61. Lorenzo, A.T.; Arnal, M.L.; Albuerne, J.; Müller, A.J. DSC isothermal polymer crystallization kinetics measurements and the use of the Avrami equation to fit the data: Guidelines to avoid common problems. *Polym. Test.* **2007**, *26*, 222–231. [CrossRef]
62. Chen, X.; Rodrigue, D.; Kaliaguine, S. Diamino-organosilicone APTMDS: A new cross-linking agent for polyimides membranes. *Sep. Purif. Technol.* **2012**, *86*, 221–233. [CrossRef]
63. Müller, A.J.; Ávila, M.; Saenz, G.; Salazar, J. Crystallization of PLA-based Materials. In *Poly(Lactic Acid) Science and Technology: Processing*; Royal Society of Chemistry: London, UK, 2014; pp. 66–100.
64. Mohapatra, A.K.; Mohanty, S.; Nayak, S.K. Properties and characterization of biodegradable poly(lactic acid) (pla)/poly(ethylene glycol) (PEG) and PLA/Peg/Organoclay. *J. Thermoplast. Comp. Mater.* **2014**, *29*, 443–463. [CrossRef]
65. Li, Y.; Li, X.; Xiang, F.; Huang, T.; Wang, Y.; Wu, J.; Zhou, Z. Crystallization, rheological, and mechanical properties of PLLA/PEG blend with multiwalled carbon nanotubes. *Polym. Adv. Technol.* **2011**, *22*, 1959–1970. [CrossRef]
66. Nagarajan, V.; Mohanty, A.K.; Misra, M. Crystallization behavior and morphology of polylactic acid (PLA) with aromatic sulfonate derivative. *J. Appl. Polym. Sci.* **2016**, *133*, 1–11. [CrossRef]
67. Michell, R.M.; Müller, A.J.; Spasova, M.; Dubois, P.; Burattini, S.; Greenland, B.W.; Hamley, I.W.; Hermida-Merino, D.; Cheval, N.; Fahmi, A. Crystallization and stereocomplexation behavior of poly(D- and L-lactide)-b-poly(N,N-dimethylamino-2-ethyl methacrylate) block copolymers. *J. Polym. Sci. Part B Polym. Phys.* **2011**, *49*, 1397–1409. [CrossRef]
68. Tarani, E.; Pušnik Črešnar, K.; Zemljič, L.F.; Chrissafis, K.; Papageorgiou, G.Z.; Lambropoulou, D.; Zamboulis, A.; Bikiaris, D.N.; Terzopoulou, Z. Cold crystallization kinetics and thermal degradation of pla composites with metal oxide nanofillers. *Appl. Sci.* **2021**, *11*, 3004. [CrossRef]
69. Yasuniwa, M.; Tsubakihara, S.; Sugimoto, Y.; Nakafuku, C. Thermal analysis of the double-melting behavior of poly(L-lactic acid). *J. Polym. Sci. Part B Polym. Phys.* **2004**, *42*, 25–32. [CrossRef]
70. Tábi, T.; Sajó, I.E.; Szabó, F.; Luyt, A.S.; Kovács, J.G. Crystalline structure of annealed polylactic acid and its relation to processing. *Express Polym. Lett.* **2010**, *4*, 659–668. [CrossRef]

71. Park, B.S.; Song, J.C.; Park, D.H.; Yoon, K.B. PLA/chain-extended PEG blends with improved ductility. *J. Appl. Polym. Sci.* **2011**, *123*, 2360–2367. [CrossRef]
72. Saravana, S.; Bheemaneni, G.; Kandaswamy, R. Effect of polyethylene glycol on mechanical, thermal, and morphological properties of talc reinforced polylactic acid composites. *Mater. Today. Proc.* **2018**, *5*, 1591–1598. [CrossRef]
73. Li, D.; Jiang, Y.; Lv, S.; Liu, X.; Gu, J.; Chen, Q.; Zhang, Y. Preparation of plasticized poly (lactic acid) and its influence on the properties of composite materials. *PLoS ONE* **2018**, *13*, e0193520. [CrossRef]
74. Iannace, S.N. Isothermal Crystallization and Chain Mobility of Poly(L-lactide). *J. Appl. Polym. Sci.* **1996**, *64*, 911–919. [CrossRef]
75. Pyda, M.; Bopp, R.C.; Wunderlich, B. Heat capacity of poly(lactic acid). *J. Chem. Thermodyn.* **2004**, *36*, 731–742. [CrossRef]
76. Vasanthakumari, R.; Pennings, A.J. Crystallization kinetics of poly(l-lactic acid). *Polymer* **1983**, *24*, 175–178. [CrossRef]
77. Marand, H.; Xu, J.; Srinivas, S. Determination of the equilibrium melting temperature of polymer crystals: Linear and nonlinear Hoffman-Weeks extrapolations. *Macromolecules* **1998**, *31*, 8219–8229. [CrossRef]
78. Karimi, S.; Ghasemi, I.; Abbassi-Sourki, F. A study on the crystallization kinetics of PLLA in the presence of Graphene Oxide and PEG-grafted-Graphene Oxide: Effects on the nucleation and chain mobility. *Compos. Part B Eng.* **2019**, *158*, 302–310. [CrossRef]
79. Avrami, M. Granulation, phase change, and microstructure kinetics of phase change. III. *J. Chem. Phys.* **1941**, *9*, 177–184. [CrossRef]
80. Zhou, W.Y.; Duan, B.; Wang, M.; Cheung, W.L. Isothermal and Non-isothermal Crystallization Kinetics of Poly(L-Lactide)/Carbonated Hydroxyapatite Nanocomposite Microspheres. In *Advances in Diverse Industrial Applications of Nanocomposites*; Reddy, B., Ed.; IntechOpen: Rijeka, Croatia, 2011; Chapter 11, pp. 231–260. [CrossRef]
81. Song, R.; Xue, R.; He, L.H.; Liu, Y.; Xiao, Q.L. the Structure and Properties of Chitosan / Polyethylene. *Polym. Sci.* **2008**, *26*, 621–630.
82. Di Lorenzo, M.L. Determination of spherulite growth rates of poly(L-lactic acid) using combined isothermal and non-isothermal procedures. *Polymer* **2001**, *42*, 9441–9446. [CrossRef]
83. Hoffman, J.D. Regime III crystallization in melt-crystallized polymers: The variable cluster model of chain folding. *Polymer* **1983**, *24*, 3–26. [CrossRef]
84. Wu, D.; Wu, L.; Wu, L.; Xu, B.; Zhang, Y.; Zhang, M. Nonisothermal Cold Crystallization Behavior and Kinetics of Polylactide/Clay Nanocomposites. *J. Polym. Sci. Part B. Polym. Phys.* **2007**, *45*, 1100–1113. [CrossRef]
85. Miyata, T.; Masuko, T. *Crystallization Behavior of Poly(L-Lactide)*; Elsevier: Amsterdam, The Netherlands, 1997; pp. 745–748.
86. Song, Y.; Wang, D.; Jiang, N.; Gan, Z. Role of PEG Segment in Stereocomplex Crystallization for PLLA/PDLA-b-PEG-b-PDLA Blends. *ACS Sustain. Chem. Eng.* **2015**, *3*, 1492–1500. [CrossRef]
87. Nazari, T.; Garmabi, H. Thermo-rheological and interfacial properties of polylactic acid/polyethylene glycol blends toward the melt electrospinning ability. *J. Appl. Polym. Sci.* **2016**, *133*, 1–11. [CrossRef]
88. Mandelkern, L. *Crystallization of Polymers*; Cambridge University Press: Cambridge, UK, 2004; pp. 217–281.
89. Zhang, J.; Wang, S.; Zhao, D.; Zhang, Y.; Pang, W.; Zhang, B.; Li, Q. Improved processability and performance of biomedical devices with poly(lactic acid)/poly(ethylene glycol) blends. *J. Appl. Polym. Sci.* **2017**, *134*, 45194. [CrossRef]
90. Chrysafi, I.; Ainali, N.M.; Bikiaris, D.N. Thermal degradation mechanism and decomposition kinetic studies of poly(lactic acid) and its copolymers with poly(hexylene succinate). *Polymers* **2021**, *13*, 1365. [CrossRef] [PubMed]
91. Zou, H.; Yi, C.; Wang, L.; Liu, H.; Xu, W. Thermal degradation of poly(lactic acid) measured by thermogravimetry coupled to Fourier transform infrared spectroscopy. *J. Thermal. Anal. Calor.* **2009**, *97*, 929–935. [CrossRef]
92. Henrique, P.; Cardoso, M.; Ferreira, M.; Oliveira, L.D.; De, M.; Mara, R. 3D Printed Parts of Polylactic Acid Reinforced with Carbon Black and Alumina Nanofillers for Tribological Applications. *Macromol. Symp.* **2020**, *394*, 2000155. [CrossRef]
93. Salleh, F.M.; Hassan, A.; Yahya, R.; Azzahari, A.D. Effects of extrusion temperature on the rheological, dynamic mechanical and tensile properties of kenaf fiber/HDPE composites. *Compos. Part B* **2014**, *58*, 259–266. [CrossRef]
94. Liu, Y.; Shao, J.; Sun, J.; Bian, X.; Feng, L.; Xiang, S.; Sun, B.; Chen, Z.; Li, G.; Chen, X. Improved mechanical and thermal properties of PLLA by solvent blending with PDLA-b-PEG-b-PDLA. *Polym. Degrad. Stab.* **2014**, *101*, 10–17. [CrossRef]
95. Zhao, P.; Liu, Z.; Wang, X.; Pan, Y.T.; Kuehnert, I.; Gehde, M.; Wang, D.Y.; Leuteritz, A. Renewable vanillin based flame retardant for poly(lactic acid): A way to enhance flame retardancy and toughness simultaneously. *RSC Adv.* **2018**, *8*, 42189–42199. [CrossRef]
96. Zhang, Q.; Mochalin, V.N.; Neitzel, I.; Hazeli, K.; Niu, J.; Kontsos, A.; Zhou, J.G.; Lelkes, P.I.; Gogotsi, Y. Mechanical properties and biomineralization of multifunctional nanodiamond-PLLA composites for bone tissue engineering. *Biomaterials* **2012**, *33*, 5067–5075. [CrossRef]
97. Alberton, J.; Martelli, S.M.; Fakhouri, F.M.; Soldi, V. Mechanical and moisture barrier properties of titanium dioxide nanoparticles and halloysite nanotubes reinforced polylactic acid (PLA). *IOP Conf. Ser. Mater. Sci. Eng.* **2014**, *64*, 012010. [CrossRef]
98. Hong, Z.; Zhang, P.; He, C.; Qiu, X.; Liu, A.; Chen, L.; Chen, X.; Jing, X. Nano-composite of poly(L-lactide) and surface grafted hydroxyapatite: Mechanical properties and biocompatibility. *Biomaterials* **2005**, *26*, 6296–6304. [CrossRef] [PubMed]
99. García, M.G.; Marchese, J.; Ochoa, N.A. Effect of the Particle Size and Particle Agglomeration on Composite Membrane Performance. *J. Appl. Polym. Sci.* **2010**, *118*, 2417–2424. [CrossRef]
100. Ashraf, M.A.; Peng, W.; Zare, Y.; Rhee, K.Y. Effects of Size and Aggregation/Agglomeration of Nanoparticles on the Interfacial/Interphase Properties and Tensile Strength of Polymer Nanocomposites. *Nanoscale Res. Lett.* **2018**, *13*, 214. [CrossRef]

101. Yang, H.Y.; Wang, Z.; Chen, L.Y.; Shu, S.L.; Qiu, F. Interface formation and bonding control in high-volume-fraction (TiC + TiB_2)/Al composites and their roles in enhancing properties. *Compos. Part B* **2021**, *209*, 108605. [CrossRef]
102. Das, K.; Ray, S.S.; Chapple, S.; Wesley-smith, J. Mechanical, Thermal, and Fire Properties of Biodegradable Polylactide/Boehmite Alumina Composites. *Ind. Eng. Chem. Res.* **2013**, *52*, 6083–6091. [CrossRef]
103. Dong, T.; Song, S.; Liang, M.; Wang, Y.; Qi, X.; Zhang, Y.; Yun, X.; Jin, Y. Gas Permeability and Permselectivity of Poly(L-Lactic Acid)/SiOx Film and Its Application in Equilibrium-Modified Atmosphere Packaging for Chilled Meat. *J. Food Sci.* **2017**, *82*, 97–107. [CrossRef] [PubMed]
104. Lee, J.S.; Kim, J.W. Effect of cooling rate on mechanical properties of carbon fibre fabric and polypropylene composites. *Mater. Res. Express* **2017**, *4*, 095304. [CrossRef]
105. Lee, W.I.; Talbott, M.F.; Springer, G.S.; Berglund, L.A. Effects of Cooling Rate on the Crystallinity and Mechanical Properties of Thermoplastic Composites. *J. Reinf. Plast. Compos.* **1987**, *6*, 2–12. [CrossRef]
106. Jia, Z.; Zhang, K.; Tan, J.; Han, C.; Dong, L.; Yang, Y. Crystallization Behavior and Mechanical Properties of Crosslinked Plasticized Poly(L-lactic acid). *Appl. Polym. Sci.* **2008**, *111*, 1531–1539. [CrossRef]
107. Huang, S.; Li, H.; Jiang, S.; Chen, X.; An, L. Crystal structure and morphology influenced by shear effect of poly(l-lactide) and its melting behavior revealed by WAXD, DSC and in situ POM. *Polymer* **2011**, *52*, 3478–3487. [CrossRef]
108. Yampolskii, Y. Polymeric gas separation membranes. *Macromolecules* **2012**, *45*, 3298–3311. [CrossRef]
109. Kathuria, A.; Al-Ghamdi, S.; Abiad, M.G.; Auras, R. The influence of $Cu_3(BTC)_2$ metal organic framework on the permeability and perm-selectivity of PLLA-MOF mixed matrix membranes. *J. Appl. Polym. Sci.* **2015**, *132*, 1–10. [CrossRef]
110. Lizundia, E.; Vilas, J.L.; Sangroniz, A.; Etxeberria, A. Light and gas barrier properties of PLLA/metallic nanoparticles composite films. *Eur. Polym. J.* **2017**, *91*, 10–20. [CrossRef]
111. Sangeetha, V.H.; Deka, H.; Varghese, T.O.; Nayak, S.K. *State of the Art and Future Prospectives of Poly (Lactic Acid) Based Blends and Composites*; Wiley Online Library: Hoboken, NJ, USA, 2016; pp. 1–21. [CrossRef]
112. Rajeshkumar, G.; Arvindh Seshadri, S.; Devnani, G.; Sanjay, M.; Siengchin, S.; Prakash Maran, J.; Al-Dhabi, N.A.; Karuppiah, P.; Mariadhas, V.A.; Sivarajasekar, N.; et al. Environment friendly, renewable and sustainable poly lactic acid (PLA) based natural fiber reinforced composites—A comprehensive review. *J. Clean. Prod.* **2021**, *310*, 127483. [CrossRef]
113. Kaseem, M.; Rehman, Z.U.; Hossain, S.; Singh, A.K.; Dikici, B. A Review on Synthesis, Properties, and Applications of Polylactic Acid/Silica Composites. *Polymers* **2021**, *13*, 3036. [CrossRef] [PubMed]